NAVAL POSTGRADUATE SCHOOL

MONTEREY, CALIFORNIA

THESIS

THE ISOTHERMAL DEFORMATION OF NICKEL ALUMINUM BRONZE IN RELATION TO FRICTION STIR PROCESSING

by

Frank Allen Pierce

June 2004

Thesis Advisor: Terry R. McNelley

Approved for public release; distribution is unlimited

THIS PAGE INTENTIONALLY LEFT BLANK

REPORT DOCUMENTATION PAGE			Form Approved OMB No. 0704-0188
Public reporting burden for this collection of information is estimated to average 1 hour per response, including the time for reviewing instruction, searching existing data sources, gathering and maintaining the data needed, and completing and reviewing the collection of information. Send comments regarding this burden estimate or any other aspect of this collection of information, including suggestions for reducing this burden, to Washington headquarters Services, Directorate for Information Operations and Reports, 1215 Jefferson Davis Highway, Suite 1204, Arlington, VA 22202-4302, and to the Office of Management and Budget, Paperwork Reduction Project (0704-0188) Washington DC 20503.			
1. AGENCY USE ONLY ***(Leave blank)***	**2. REPORT DATE** June 2004	**3. REPORT TYPE AND DATES COVERED** Master's Thesis	
4. TITLE AND SUBTITLE: The Isothermal Deformation of Nickel Aluminum Bronze in Relation to the Friction Stir Processing			**5. FUNDING NUMBERS**
6. AUTHOR(S) Pierce, Frank A.			
7. PERFORMING ORGANIZATION NAME(S) AND ADDRESS(ES) Naval Postgraduate School Monterey, CA 93943-5000			**8. PERFORMING ORGANIZATION REPORT NUMBER**
9. SPONSORING /MONITORING AGENCY NAME(S) AND ADDRESS(ES) N/A			**10. SPONSORING/MONITORING AGENCY REPORT NUMBER**
11. SUPPLEMENTARY NOTES The views expressed in this thesis are those of the author and do not reflect the official policy or position of the Department of Defense or the U.S. Government.			
12a. DISTRIBUTION / AVAILABILITY STATEMENT Approved for public release; distribution is unlimited			**12b. DISTRIBUTION CODE**

13. ABSTRACT (maximum 200 words)

The extreme strain, strain rate and temperature gradients during Friction Stir Processing (FSP) render measurement of key parameters in the "stir zone" infeasible with common methods. The objective of this research was to separate the effects that temperature and deformation in an experimental study of the microstructure and mechanical properties of Ni-AL bronze (NAB). This was accomplished by subjecting as-cast NAB material to several isothermal annealing and quenching treatments as well as isothermal hot rolling processes. Sufficient material was generated to provide results and data for subsequent optical microscopy, tensile, & hardness tests. All results were then compared to similar data collected from previous works completed here at Naval Postgraduate School and with other DARPA FSP program participants. During the course of this work correlations were drawn between FSP material and the material subjected to isothermal hotworking, which may enhance our understanding of the roles that various FSP process parameters have on the microstructural transformation sequence within this material. The hot-rolling study conducted here suggests that FSP process parameters leading to severe deformation at temperatures between 950-1000ºC in the NAB material provides high ductility (elongation ~ 28%) with moderate strengths.

14. SUBJECT TERMS Friction Stir Processing, Nickel-Aluminum Bronze, NAB, Isothermal Deformation, Annealing, Optical Microscopy, Naval Propellers, Surface Treatment, Thermomechanically Affected Zone, Shear Deformation, Homogenization of Microstructure, Grain Refinement			**15. NUMBER OF PAGES** 71
			16. PRICE CODE
17. SECURITY CLASSIFICATION OF REPORT Unclassified	**18. SECURITY CLASSIFICATION OF THIS PAGE** Unclassified	**19. SECURITY CLASSIFICATION OF ABSTRACT** Unclassified	**20. LIMITATION OF ABSTRACT** UL

NSN 7540-01-280-5500 Standard Form 298 (Rev. 2-89)
Prescribed by ANSI Std. 239-18

THIS PAGE INTENTIONALLY LEFT BLANK

Approved for public release; distribution is unlimited

THE ISOTHERMAL DEFORMATION OF NICKEL ALUMINUM BRONZE IN RELATION TO FRICTION STIR PROCESSING

Frank A. Pierce
Lieutenant, United States Coast Guard
B.S., United States Coast Guard Academy, 1997

Submitted in partial fulfillment of the
requirements for the degree of

MASTER OF SCIENCE IN MECHANICAL ENGINEERING

from the

NAVAL POSTGRADUATE SCHOOL
June 2004

Author: Frank Allen Pierce

Approved by: Terry R. McNelley
Thesis Advisor

Anthony J. Healey
Chairman, Department of Mechanical and Astronautical Engineering

THIS PAGE INTENTIONALLY LEFT BLANK

ABSTRACT

The extreme strain, strain rate and temperature gradients during Friction Stir Processing (FSP) render measurement of key parameters in the "stir zone" infeasible with common methods. The objective of this research was to separate the effects that temperature and deformation in an experimental study of the microstructure and mechanical properties of Ni-AL bronze (NAB). This was accomplished by subjecting as-cast NAB material to several isothermal annealing and quenching treatments as well as isothermal hot rolling processes. Sufficient material was generated to provide results and data for subsequent optical microscopy, tensile, & hardness tests. All results were then compared to similar data collected from previous works completed here at Naval Postgraduate School and with other DARPA FSP program participants. During the course of this work correlations were drawn between FSP material and the material subjected to isothermal hotworking, which may enhance our understanding of the roles that various FSP process parameters have on the microstructural transformation sequence within this material. The hot-rolling study conducted here suggests that FSP process parameters leading to severe deformation at temperatures between 950-1000ºC in the NAB material provides high ductility (elongation ~ 28%) with moderate strengths.

THIS PAGE INTENTIONALLY LEFT BLANK

TABLE OF CONTENTS

LIST OF FIGURES

THIS PAGE INTENTIONALLY LEFT BLANK

LIST OF TABLES

THIS PAGE INTENTIONALLY LEFT BLANK

ACKNOWLEDGMENTS

The author would like to thank the Defense Advanced Research Projects Agency – Dr. Leo Christodoulou for their support of this research; Mr. Bill Palko and Dr. David Forrest at the Naval Surface Warfare Center – Carderock Division for the NAB material and additional testing support. Also thanks to Mr. Murray Mahoney and his crew at the Rockwell Scientific Center, Thousand Oaks, CA for material support and the chance to get a glimpse of future with a tour of their facility.

Special thanks to Professor Terry McNelley for sharing his knowledge. Somehow he remained patient and understanding through the entire learning process.

Thanks to Dr. Chanman Park, Dr. Keiichiro Oishi, and Dr. Alex Zhilyaev for pushing me in the right directions.

To Deanna with love - Thank you so much for our son Luke, and for handling all of the work that I laid on you during this process; I couldn't have done it without your love and support.

THIS PAGE INTENTIONALLY LEFT BLANK

I. INTRODUCTION

A. OVERVIEW

The ability to strengthen materials through repeated thermal treatments and deformation processes has long since been recorded. Even today new and innovative fabrication techniques are continuously being developed to take advantage of these concepts. Among these techniques, Friction Stir Processing (FSP) is gaining attention as a new bulk or even post processing method to perform highly selective modifications on materials without producing significant distortion to the materials original shape. Many of these complex fabrication techniques rely heavily on empirical data to refine and finalize process controls and parameters. Now, in a time where computing power is cheaper than the time required for testing and materials, studies and experiments are instead being used to hone and validate more cost effective numerical models. In a program funded by the Defense Advanced Research Projects Agency, the research being conducted at the Naval Postgraduate School in collaboration with other program participants aims to provide the microstructural analysis and related characterization studies to provide the foundation necessary to help commercialize FSP, and, in particular, for the technique to be used in the post processing of U.S. Navy propeller castings.

B. FRICTION STIR PROCESSING

Friction Stir Processing (FSP) is an adaptation of the solid state joining process of Friction Stir Welding (FSW) discovered and patented by TWI, Ltd., in 1991 [Ref. 1]. Investigations into the microstructural and mechanical characteristics of the FSW joints in several different alloys ultimately revealed a refined and homogenized microstructure [Ref. 2,4]. In many ambient temperature applications the wrought condition created by the FSW to the material lead to significant increases in the properties of strength and toughness which then brought about FSP [Ref. 2]. Secondary benefits for some materials include superplasticity effects, better weldability and improved fatigue/corrosion resistance [Ref 3].

FSP is considered a hot working process in which extreme strain, strain rate and thermal gradients are imposed over a small volume of material [Ref. 4]. These conditions are achieved through the use of a non-consumable tool that, simply stated, is rotated, pressed into and traversed through a material under specified process conditions. The process parameters and material conditions are defined with definitions borrowed from welding processes. In common with welding processes, FSP shares the concept of a "heat affected zone" (HAZ), however the term thermomechanically affected zone (TMAZ) is often used because of the localized hotworking that also occurs [Ref. 4]. In some locations peak temperatures (T_{peak}) reach > 0.9 T_{melt} although melting is not observed. Features not common with welding that are immediately apparent in FSP are the "stir zone" (SZ), also known as the "stir nugget". Unlike welding, FSP does not have a fusion zone because it is believed that this process remains entirely in the solid-state [Ref. 1-4]. In Figure 1, a micrograph that captures a transverse section of FSP nickel-aluminum bronze. This figure depicts the two zones, SZ and TMAZ, relative to the base metal. FSP process parameters and tool terminology used primarily for control of FSP are illustrated below in Figures 2 and 3.

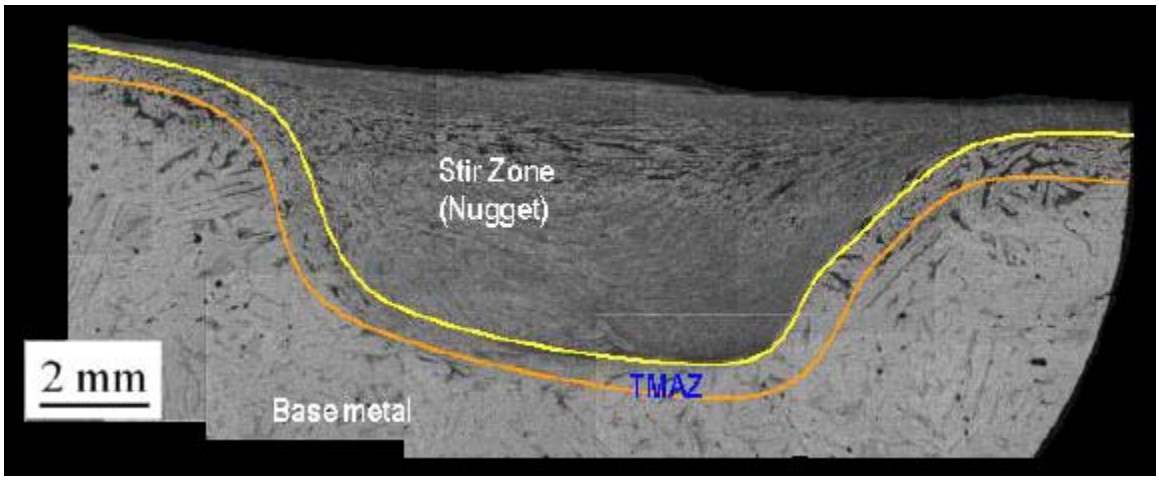

Figure 1. Example of FSP Region (courtesy of Dr. K. Oishi, NPS)

Figure 2 describes the FSP process. Figure 2 (a) shows that the tool is rotated a predetermined speed (RPM) prior to penetration. Next, as shown in Figure 2 (b) the tool

is lowered until the pin is in contact with the material surface. This contact creates frictional heating as a function of axial force, RPM of the tool. The axial force is held constant and results in the pin penetrating the surface as the heated zone expands and material softens. Eventually the penetration will allow the shoulder to make contact, Figure 2 (c), resulting in further expansion of the heated zone. Shoulder contact will also restrict further penetration for a set axial force. The tool is ready to be traversed, Figure 2 (d) in the travel direction (IPM) along the surface.

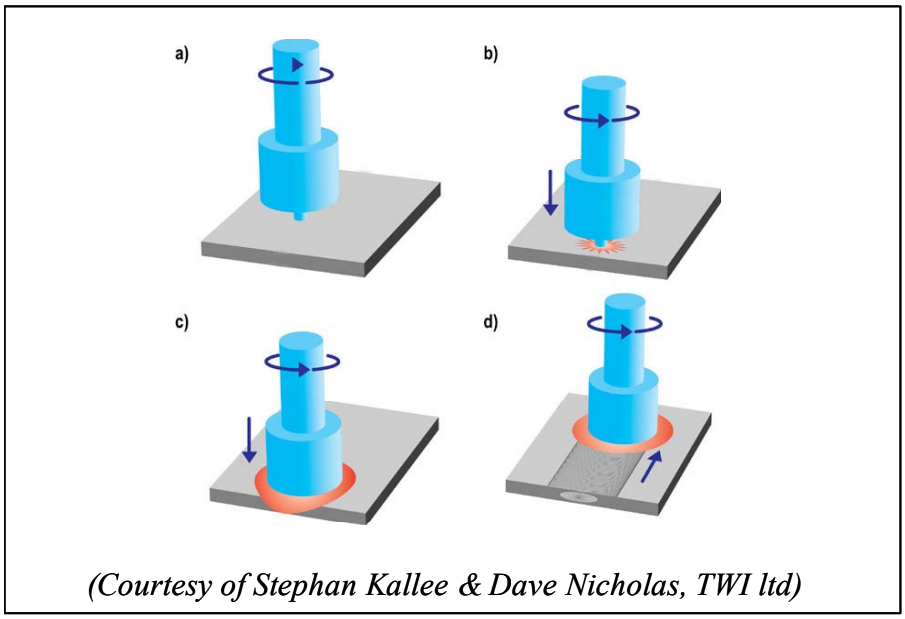

Figure 2. Friction Stir Process Illustration (adapted from [Ref. 1])

Figure 3 depicts FSP terminology used to describe the process. In Figure 3, the major features of the tool geometry are the shoulder diameter and pin length as well as its diameter. Further parameters can include the pin shape. Diameters for the tool shoulders and pins vary from a few millimeters to a few centimeters. Pin lengths for these tools can vary up to 100% of their diameter, depending on the material. The pin is always concentric to the shoulder. The size and shape of the "Stir Zone" (SZ) and the resulting flow within the stir zone are closely related to tool geometry. Figure 3 also depicts material flow within the SZ as a result of a tool pin that contains grooves. The sense of rotation defines the advancing and retreating sides of the "Stir Zone". The advancing side is where the apparent speed of the rotation direction on the outer radius of the tool in

conjunction with the travel/traversing direction results in the greatest relative speed between the tool and the material. The advancing side is always orthogonal to the travel/traversing direction of the tool. The retreating side is opposite to the advancing side and applies to the lowest relative speed between the tool and material. Speed of the tool rotation is referred to as revolutions per minute (RPM). The travel direction is the direction the rotational axis of the tool traverses and this is not restricted to straight lines. Rastering and multi-passes through materials are also possible. The speed or traverse rate of the tool is referred to as inches per minute (IPM). The axial force is applied inline with the rotational axis and nearly normal to the surface of the material; the tool axis is generally be inclined in the travel direction to minimize tool-induced defects.

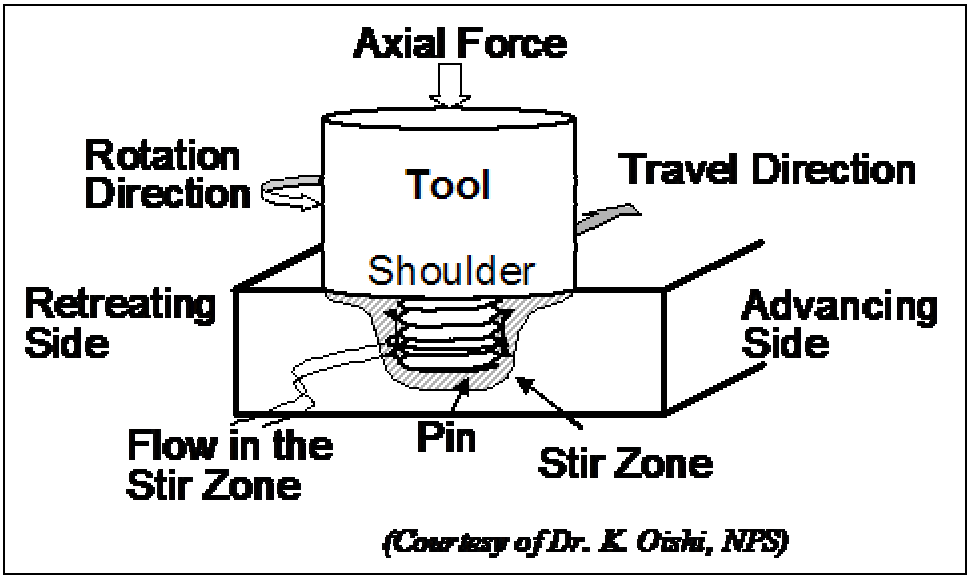

Figure 3. Friction Stir Terminology Diagram (courtesy of Dr. K. Oishi, NPS)

Friction Stir Processing is unique in its processing advantages. The tool is essentially non-consumable and may last over total lineal distances of up to 1000 m, depending on parameters, and this may represent a surface area of up to 30 m^2 [Ref. 1]. Processing requires no filler wire or shielding gases. Additionally, very little material preparation is required because light to moderate oxide layers are, in most cases, acceptable [Ref. 1]. The process is very efficient, produces almost no distortion (at least for a single pass) and, aside from some required keyholing (run-in, run-out tabs), leaves

the material with almost same as the starting geometry. Characterization of the SZ, TMAZ, and base metal interfaces for various materials and process parameters has been an ongoing process. The complex strain, strain rate and temperature histories are a result of the plastic flow caused by the intense shear and the tool's stirring action. This complex microstructural history requires a systematic approach to achieve understanding of the mechanistic principles behind this new process and to aid in interpretation of microstructural constituents such as lamellar, banded or spheroidized structures, and other features including various particles, tunneling, onion ring structures and the existence of very fine grains found in processed nickel-aluminum bronze. There have been many investigations into the benefits and effects observed in FSP and FSW since 1991; however on-going research is needed to help refine modeling algorithms and process parameters. These include RPM, IPM and tool geometry that is still great part of research conducted including the work presented in this thesis.

C. NICKEL ALUMINUM BRONZE (NAB)

Nickel-aluminum bronze (NAB), which, for certain compositions, is also known as "propeller bronze," gained its popularity for marine applications because it exhibits a unique combination of properties that include moderate strength and toughness coupled with excellent fatigue, corrosion, cavitation and erosion resistance [Ref. 5-6]. These desirable properties have led to the nickname "propeller bronze". Propeller bronzes are Copper (Cu) based alloys with intentional additions of Aluminum (Al), Nickel (Ni), Iron (Fe) and Manganese (Mn). Percentages of the alloying elements can vary, but fall under the specification ASTM B 148-78 designation C95800 [Ref. 7]. Table 2 in Chapter III contains specific composition information regarding C95800, and alloy compositions attained from separately run X-ray dispersion fluorescence analyses for each alloy used in this research.

Due to their immense size, ship propeller castings and the casting process itself lowers the overall values of the mechanical properties when compared with wrought material. Propeller casting requires many months of post-cast processing to render these propellers fit for sea service [Ref. 8]. The massively thick sections in propeller casts involve very slow cooling as well as large variations in cooling rate [Ref. 9]. Therefore

the cooling rates experienced from pouring temperatures (T_{melt}) to ambient ($T_{ambient}$) are small ($10^{-3}C \bullet s^{-1}$) and more than one week is required to cool to ambient temperature. Many investigations into the effects of slow cooling of propeller casts have shown that degradation in properties is directly attributable to related phase changes in conjunction with grain coarsening [Ref. 5, 9]. Post casting heat treatments have been attempted to mitigate the phase structure changes and segregation effects. In general, heat treatments can alter the material microstructure to obtain more desirable properties but such treatments do not remove other casting defects such as porosity [Ref. 5, 9]. The treatments themselves have also been noted to promote an overall decrease in ductility [Ref. 5]. Surface and sub-surface porosity remains an issue, and, when necessary, is currently rectified with a costly inspection, weld repair and re-inspection process. Welding repairs to correct porosity currently use a "buttering" technique that can introduce further thermal stress and microstructural changes [Ref. 8]. This repetitive method for cast porosity repair can introduce lead times of 18 months in propeller manufacture. In comparison, FSP would be applied using a rastering method than can be used to either selectively treat regions or the entire cast surface. Aside from the mechanical property increases, the advantage that FSP offers is the removal for much of the repetitive repair process associated with closing porosity. The benefit of FSP has been projected to lower post-cast processing time from 18 to perhaps as little as three months.

D. NAB PHASES

It is useful to review the various phases that form upon cooling of NAB. The phase characteristics, properties and compositions were important to understanding how the transformation sequence of these phases might have occurred during the temperature and deformation sequence of this study. Below is a literature review regarding the various phases.

1. Beta (β) and Retained-Beta (β')Phases

The β phase is the high temperature solid solution phase of NAB. Beta has a BCC structure at high temperatures with a lattice parameter equal to 0.3568 nm. However, β is not a stable phase at ambient temperatures. Various β-transformation

products form as a result of cooling. The diagram in Figure 4 depicts the various transformations that occur during cooling of material containing the β. These products, alpha (α), and various kappa (κ) phases, are discussed in the following sections. On the left hand side of Figure 4 the transformations resulting from equilibrium cooling at very slow rates (such as those found in casting) are summarized. These slow cooling rates result in full β transformation to α and various κ phases. On the right hand side of Figure 4 it is shown that, starting from various peak temperatures (T_{peak}) and cooling at higher rates, β will decompose into a more complex series of constituents that include Widmanstätten α, coarser to finer bainite structures or β', i.e., a martensitic form. Also, a high density of precipitates form throughout the β on cooling; these particles may serve as nucleation sites for the formation of the primary α [Ref 11]. In this study, the term β transformation products will be used to refer to an entire group of different β products that form as a result of more rapid cooling of NAB, e.g., as occurs after FSP. These β transformation products will appear typically as the darker etched regions in micrographs later in this thesis. The β composition will vary depending on the amount of the alloying elements that are incorporated into other phases such as the various precipitate particles that form from solution.

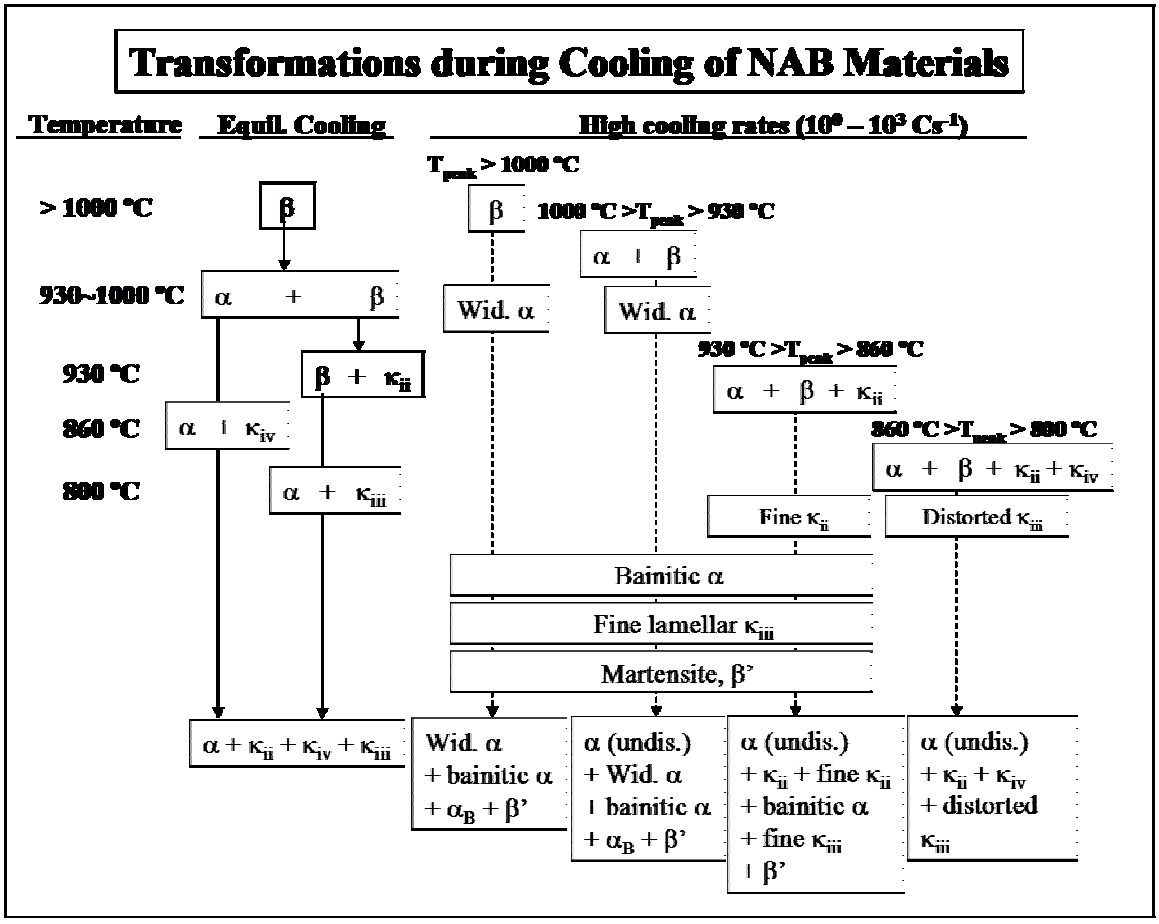

Figure 4. Transformation of NAB Phases during Cooling of NAB Materials (courtesy of Prof. Terry McNelley, NPS)

2. Alpha (α) Phase

The alpha phase is the terminal solid solution phase for NAB alloys. It is FCC with a lattice parameter of 0.364 nm [Ref. 10]. At nearly all cooling rates the alpha phase is the first to form from β upon cooling. The temperature at which this phase forms is highly dependent on composition [Ref. 11-13]. The temperatures suggested from previous work in this laboratory are indicated in Figure 4. The composition of the alpha phase (shown in Table 1) varies during the cooling process as elements are transferred at the alpha/beta boundaries and from within beta to form additional phases.

3. Kappa Phases (κ)

There are four different κ phases that form in NAB of the composition being studied, all of which are stable at ambient temperatures. These phases form as a result of the decreasing solubility of the Fe, Al, and Ni during the cooling process. These phases

can play an important role in the transformation sequence. There is value in understanding these precipitate structures, their compositions and characteristics.

The first kappa phase (κ_I), when present, is usually fully surrounded by α. This phase will generally occur in NAB compositions where the Fe content is 5% or greater and may begin forming in the melt [Ref. 11]. The κ_I precipitates are mostly iron rich (Fe_3Al, FeAl) and surround small Cu-rich particles. The composition varies as shown in Table 1 as does the crystal structure (BCC, DO_3 or B2). When present, κ_I exhibits a large rosette shape 20 to 50 microns in diameter and will etch gray in a micrograph [Ref 10].

The second kappa phase (κ_{II}) precipitate is Fe-rich (Fe_3Al) and has a DO_3 lattice structure [Ref 11]. The κ_{II} particles begin to nucleate in the β phase near α/β interfaces. These particles can be found enveloped by the α phase at ambient temperatures and are usually between 5 and 10 microns in diameter [Ref. 10]. These particles tend to form at around the same temperature region as the Widmanstätten α during transformation of β. The κ_{II} precipitates, like κ_I, etch to appear gray in the micrographs contained in this study. The approximate composition for this phase is in Table 1.

The κ_{III} phase is the only precipitate that is Ni-rich (NiAl) and has a B2 lattice structure [Ref. 10]. This phase begins to form on cooling below ~800ºC [Ref. 11]. Those alloys with the highest nickel content will tend to form the most $\kappa_{III;}$ it's approximate composition can also be found in Table 1. This phase will appear in either a globular or lamellar form for the more slowly cooled NAB microstructures; otherwise its presence is very hard to verify using optical microscopy because etching tends to readily attack the κ_{III} phase.

The κ_{IV} phase has an interatom spacing nearly identical to that of κ_{II}. The κ_{IV} particles are usually found distributed throughout the α grains except in a precipitate free zone surrounding primary α grains [Ref. 10,11] . The κ_{IV} composition is located in Table 1

Phase	Cu	Al	Ni	Fe	Mn
Alpha	85.4	8.3	2.5	2.7	1.4
Beta	85.2	8.7	3.5	1.6	1
Kappa I	8.4	17.5	3	65.6	2.7
Kappa II	9.3	22.2	6.6	53	1.9
Kappa III	12	44.3	31.5	10.2	1.6
Kappa IV	2	18.9	6.1	63.8	2.1
Alloy (Ref. 11)	**80**	**9.4**	**4.9**	**4.4**	**1.2**
*** Wt. Percent data from a similar NAB composition**					

Table 1. Chemical Analysis of Phases Present in NAB (adapted from [Ref. 13,15])

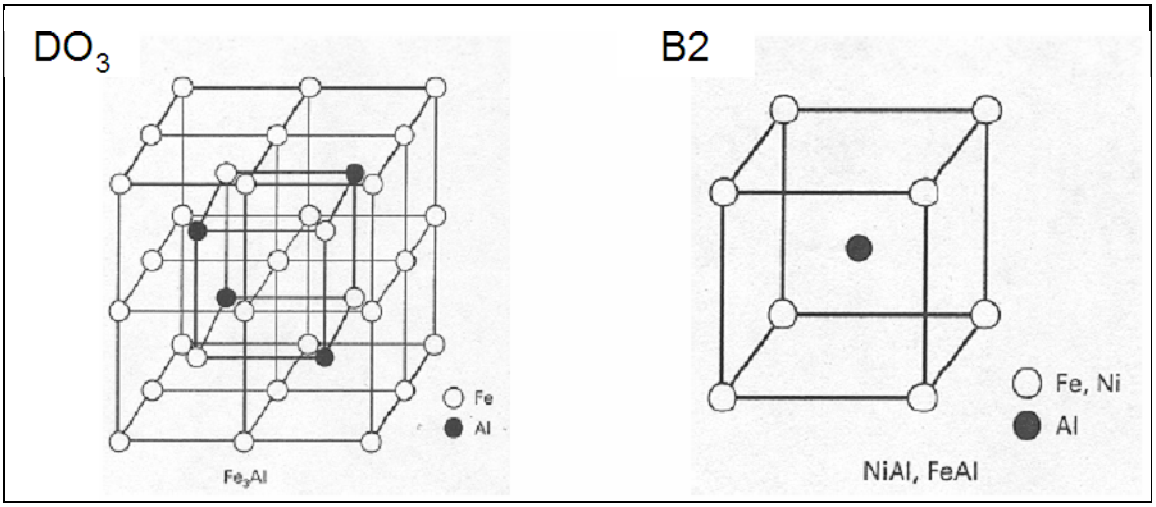

Figure 5. NAB Kappa Phase Structures (From Ref. 10)

II. OBJECTIVES OF THIS RESEARCH

The extreme strain, strain rate and temperature gradients during Friction Stir Processing (FSP) render measurement of key parameters within the SZ such as temperature and strain with standard methods unfeasible. The severity of the deformation results in distinct regions where thermomechanical history is difficult to characterize through microscopy analysis alone. The objective of this research was to separate the effects that temperature and deformation in an experimental study of the microstructure and mechanical properties of NAB. This was accomplished by subjecting as-cast NAB material to several isothermal annealing and quenching treatments as well as isothermal hot rolling processes. Sufficient material was generated to provide results and data for subsequent optical microscopy, tensile, & hardness testing. Specifically results from the annealing study were used to determine the difference between the effects of slow cooling in cast materials with faster cooling rates (e.g. air cooling or water quenching) such as those experienced during FSP. Conventional hot rolling was used to subject material to temperature and deformation histories through a succession of passes for comparison of results with materials thought to have deformed at similar peak temperatures during FSP. Tensile, macro and microhardness testing was used to assess the impact of the experiment on mechanical properties for the various material treatments. All results were then compared to similar data collected from previous works completed here at Naval Postgraduate School and with other DARPA FSP program participants. During the course of this work correlations were drawn between FSP material and the material subjected to "isothermal" hotworking, which may enhance our understanding of the roles that various FSP process parameters have on the microstructural transformation sequence within this material.

THIS PAGE INTENTIONALLY LEFT BLANK

III. EXPERIMENTAL PROCEDURES AND TESTING

A. MATERIAL & COMPOSITION

A portion of an as-cast nickel aluminum bronze (NAB) prototype propeller hub was provided by the Naval Surface Warfare Center, Carderock Division (NSWC-CD). The material was irregular in shape and the largest attainable rectangular volume was measured at 380 mm in length by 300 mm in width and 52 mm in depth. The as received material is shown in both Figures 6 and 7. The as received material was in good condition with a rough finish over the entire surface area with the exception of a small portion that was part of the casting exterior. The rough surface finish appeared to be a product of the abrasion cutting used to section the material for shipment. Minor flash rusting was observed but was not considered to have damaged any of the material.

The chemical analysis for this material was obtained from ANAMET Laboratories Inc., in Hayward, CA. The accepted nominal composition, composition data for material used in previous research (designated Alloy 1) and the data for material used in the current research (designated Alloy 2) are contained in Table 2. The iron and aluminum content in Alloy 2 exceeds the accepted composition limits. The nickel content is also higher when than the value measured in Alloy 1.

Element	Cu	Al	Ni	Fe	Mn	Si	Pb
Min-max	(min)79.0	8.5-9.5	4.0-5.0	3.5-4.5	0.8-1.5	0.10(max)	0.03(max)
Nominal	81	9	5	4	1	-	-
Alloy 1	81.2	9.39	4.29	3.67	1.20	0.05	<0.005
Alloy 2	79.26	9.80	4.71	4.95	1.01	0.08	0.01

Table 2. Composition (wt.%) of UNS C95800 NAB & Research Material (adapted from [Ref. 16])

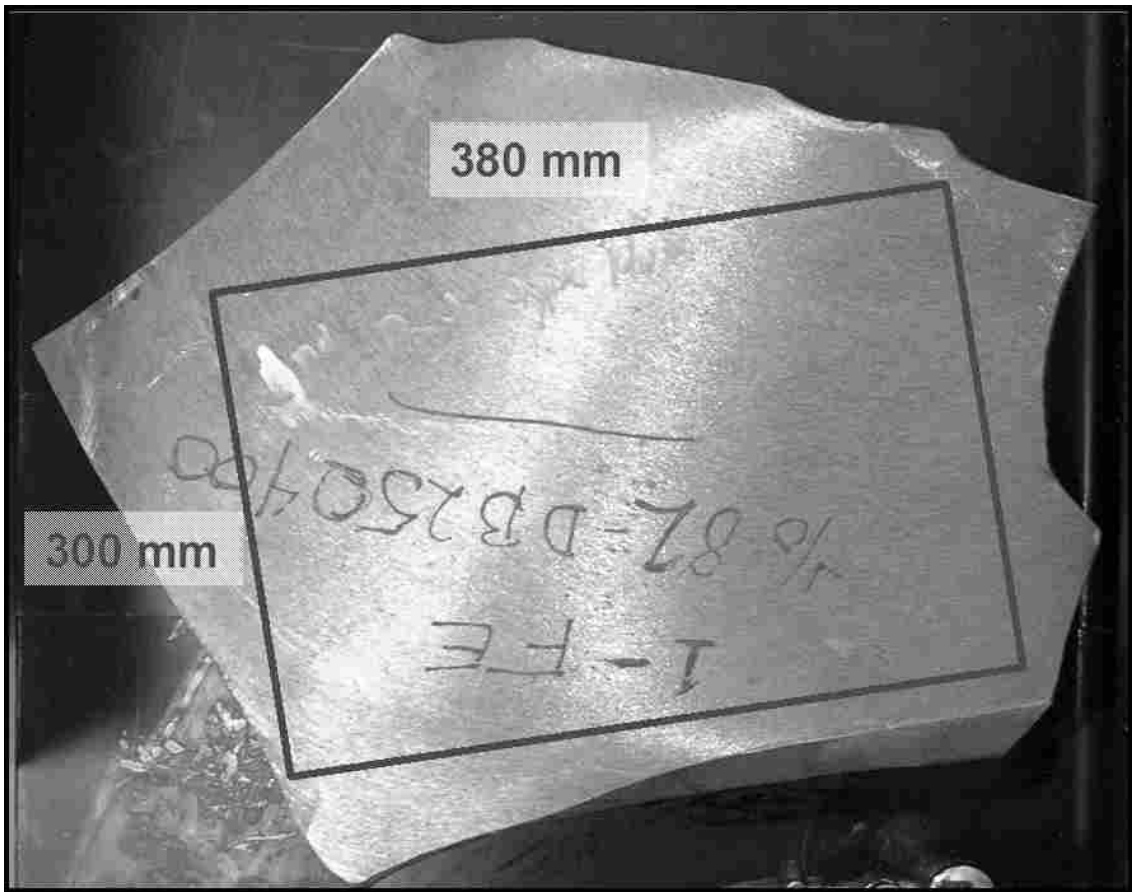

Figure 6. As Received As-Cast NAB Section of Prototype Hub (Top View)

Figure 7. As Received As-Cast NAB Section of Prototype Hub (SideView)

B. SAMPLE & TENSILE TEST SPECIMEN SECTIONING

All material was sectioned using a Charmilles Andrew EF630 electric discharge machine (EDM) using consumable brass cutting wire with a nominal diameter of 0.10 mm. The advantage of using the EDM over diamond wafering or abrasive cutting is the ability for the machine to cut out the complex geometries without imparting large external forces or excessive heat which may alter the material condition. The EDM also minimizes the amount of waste material. The ability to tightly control the cutting lines also helped to increase confidence in the tensile testing results. The photographs in Figure 5 show various steps of the material being sectioned.

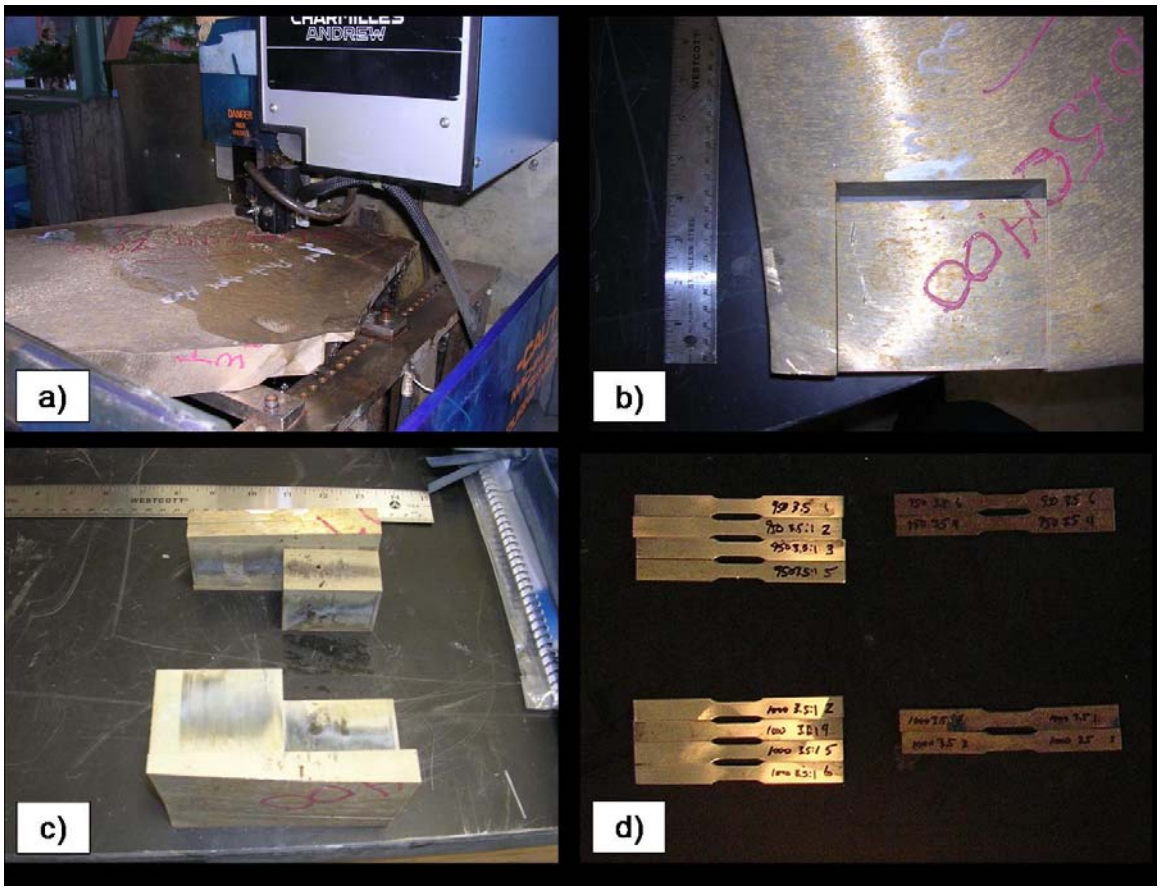

Figure 8. Sectioning as Received Material for Processing

C. ISOTHERMAL ANNEALING AND DEFORMATION

1. Annealing Treatment Procedure

Sectioned materials were subjected to isothermal annealing treatments which mirrored those preformed in previous studies by Sherburn and Vasquez [Ref 17, 18]. The Lindberg Blue-M Electric Furnace Model 51442 (Max. Temp. 1200 C) was used for these treatments. Upon the furnace reaching the isothermal annealing temperature samples were heated for 1 hour and then air cooled. Temperatures investigated were 870, 900, 950 and 1000 C. The installed furnace thermocouple readings were checked with a hand held K-type thermocouple to verify temperature accuracy. No adjustments to the furnace were necessary.

2. Deformation Procedure

Material was sectioned for conventional rolling as outlined in the schedule of Table 3. The equipment was cleaned and check for accuracy prior to use. All equipment used for measurement of the rolling process is outlined in Table 4. Rolling billets were measured prior to their 1 hr annealing treatment. After being held at temperature for 1 hour the billets were rolled using reductions no exceeding a 10% reduction in thickness per pass. The rolling mill was started 1 min prior to rolling operations to ensure smooth and even roll speeds. After each pass and before replacement into the furnace samples were rotated, flipped over and thicknesses were measured and recorded. All samples were removed from furnace and rolled within 3 seconds. Samples were replaced in the furnace within 45 seconds. After each pass, samples were brought to the process temperature and held for 5 minutes before the next pass. After the last pass, the as-rolled and final thicknesses were recorded after air cooling to room temperature.

Billet #	Temperature (Celsius)	Final Roll Reduction	Nominal Billet Dimensions (Before Rolling)
1	870	3.5 : 1	110 mm x 40 mm x 10 mm
2	900	3.5 : 1	110 mm x 40 mm x 10 mm
3	950	3.5 : 1	110 mm x 40 mm x 10 mm
4	1000	3.5 : 1	110 mm x 40 mm x 10 mm
5	870	10 : 1	55 mm x 40 mm x 30 mm
6	900	10 : 1	55 mm x 40 mm x 30 mm
7	950	10 : 1	55 mm x 40 mm x 30 mm
8	1000	10 : 1	55 mm x 40 mm x 30 mm

Table 3. Billet Temperatures, Reductions and Dimensions

Equipment Name	Equipment Description	Measurement Type – Range
Box Type Furnace	Blue-M Electric Illinois USA; Stabil-Glow Model No. 8655F-3; 240 Volt, 3 Phase, 60 Hz (44 A per phase)	Temperature – Ambient to 1200 C
Rolling Mill	The mill is two-high, Steel Hot rolls 4 inches in diameter and 6 inches wide; Manufacturer FENN, Hartford Connecticut ; 5 HP-3 PH-220/440 Volts; Variable Speed-Belt – Max. Roll Spacing- 1.25 inches	Roll Spacing approx. 1/8 inch per 1 revolution
Handheld Micrometer/Caliper	NSK	Inches 0 - 6 inches, 0.001 increments
Handheld Thermocouple	K-Type	Temperature – K-Type Thermocouple

Table 4. Equipment Description for Isothermal Rolling

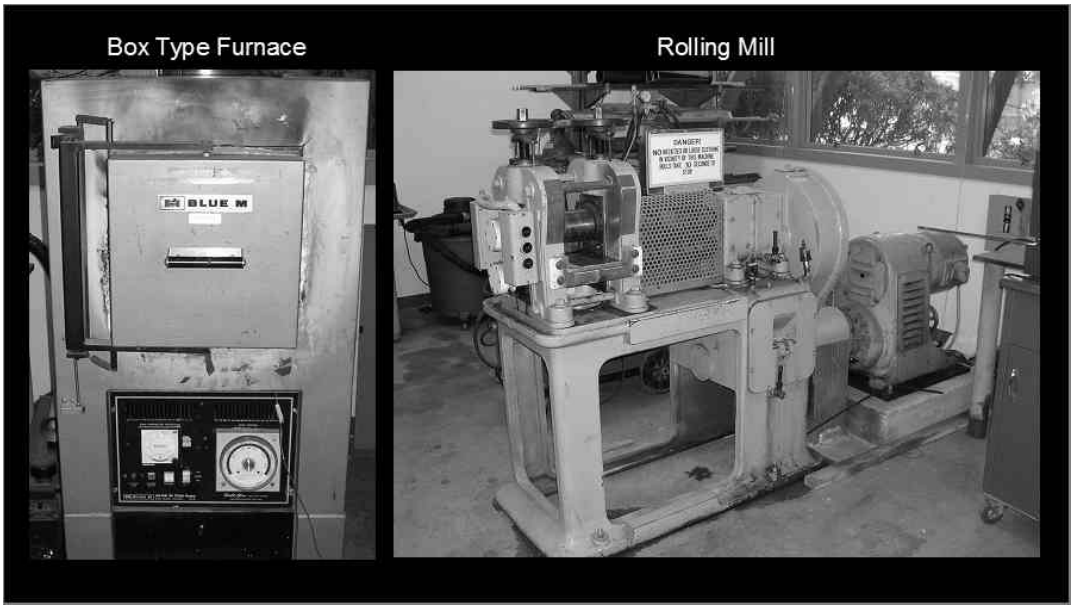

Figure 9. Isothermal Rolling Equipment Lab

D. TENSILE TESTING

Tensile test specimens were fabricated from as-cast, annealed and as-rolled material using the EDM machine. The final dimensions differed from those in tests preformed by Vasquez because of lessons learned during previous tensile testing [Ref. 17]. The shorter gauge length was still created within the guidelines of ASTM E8 for sub-size specimens. Specimen dimensions can be found in Figure 10.

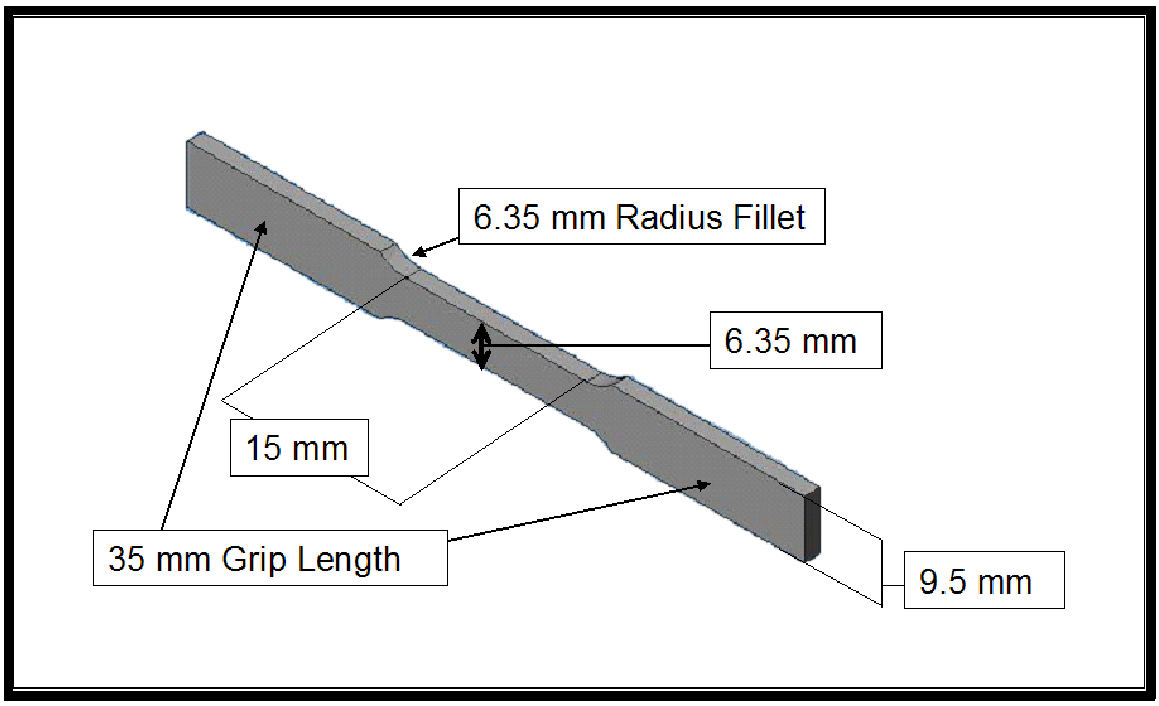

Figure 10. Tensile Specimen Dimensions

The machine used to perform the tensile testing was an INSTRON Model 4507 which was computer-operated with GPIB interface control and the Series IX data collection software. Using a standard tensile test method with a constant cross head displacement speed the specimens were loaded to failure. A 12.5 mm gauge length extensometer was used to measure engineering strains up to 0.06 before shifting to cross head displacement data. Care was exercised to properly align each sample during mounting into the wedge type grips. A universal joint was also added between the load cell and the upper grip to aid in tensile load alignment. Prior to each test the load cell,

extensometer and extension length were reset, balanced and calibrated at the INSTRON control panel. During each test engineering stress, engineering strain, load cell, strain gauge and crosshead displacement data were gathered at 5 Hz and recorded in an ASCII 2 formatted file. Data were then imported into MATLAB Version 6.5 for analysis. Data clean-up was required for 25 of the approximately 120 samples tested. Failing to properly set-up the software test method caused the data capturing error. This resulted in a loss of computer measured crosshead displacement data. The software test method was corrected immediately. Data clean-up for these 25 samples was completed using the data logging rate of 5 Hz and the known constant cross head displacement rate of 0.762 mm/min. to generate the missing displacement data. The data generated for displacement using this method fit well with the extensometer data, however the new curves did not exhibit the relaxation spike from extensometer removal that was observed in the remaining tensile tests. All other tensile testing errors such as slippage were considered failures and were removed from the data sample set.

E. ROCKWELL HARDNESS TESTING

Macrohardness data was recorded for all conditions of the Alloy 2 material. The machine used for testing was manufactured by WILSON model number 1JR using the B-scale; 100 kg weight and 1/16" ball indenter. A test block was used to properly seat the indenter and test machine accuracy. The average of five readings was taken from as-cast, annealed and deformed material. Statistical outliers were not included in the five readings and such samples were re-tested.

F. SAMPLE PREPARATIONS

Samples of as-cast, annealed and hotworked material were mounted in 1.25 inch premold - red phenolic using a Buehler SIMPLIMET 2 mounting press. Rolled sample materials were oriented so that the plane defined by the rolling direction (RD) and normal direction (ND) were viewable for all analysis and testing. The rolled material was sectioned with a higher length-to-thickness aspect ratio for ease in the identification of RD/ND axes. Mounted samples were then mechanically polished following the schedule outlined in Table 5 for the indicated conditions using both Buehler ECOMET 4 and

ECOMET 3 polishing wheels combined with the Buehler AUTOMET 2 powerhead. After polishing steps 6 – 9 the samples were ultrasonically cleaned in methanol. In the case where the samples were prepared for optical microscopy the samples were etched in a dilute 10% ammonium persulfate solution for 15 secs. In the case where samples were prepared for testing with orientation imaging microscopy (OIM) in the TOPCON SM-510 Scanning Electron Microscope (SEM), samples were mounted in PROBEMET conductive molding compound using the same procedures.

Step	Abrasive	Time	RPM	Force
1	320 Grit SiC Paper	10 min.	150	5 lbs
2	500 Grit SiC Paper	10 min.	150	5 lbs
3	800 Grit SiC Paper	5 min.	150	5 lbs
4	1000 Grit SiC Paper	5 min.	150	5 lbs
5	2400 Grit SiC Paper	5 min.	150	5 lbs
6	4000 Grit SiC Paper	5 min.	150	5 lbs
7	3 micron Metafi Diamond Suspension	5 min.	90	2 lbs
8	1 micron Metafi Diamond Suspension	5 min.	90	2 lbs
9	0.05 micron Colloidal Silica	5 min.	90	2 lbs

Table 5. Mechanical Polishing Schedule

G. OPTICAL MICROSCOPY

Optical microscopy was conducted using a Carl Zeiss JENAPHOT 2000 reflected light photomicroscope, with output via a PULNIX TMC-74 – CCD Camera (Figure 11). The digital output of the camera was used with SEMICAPS photo capturing and measurement software. Micrographs were prepared for all as-cast and treated materials of the Alloy 2 composition (see Table 2) for analysis and comparison with previous NAB studies.

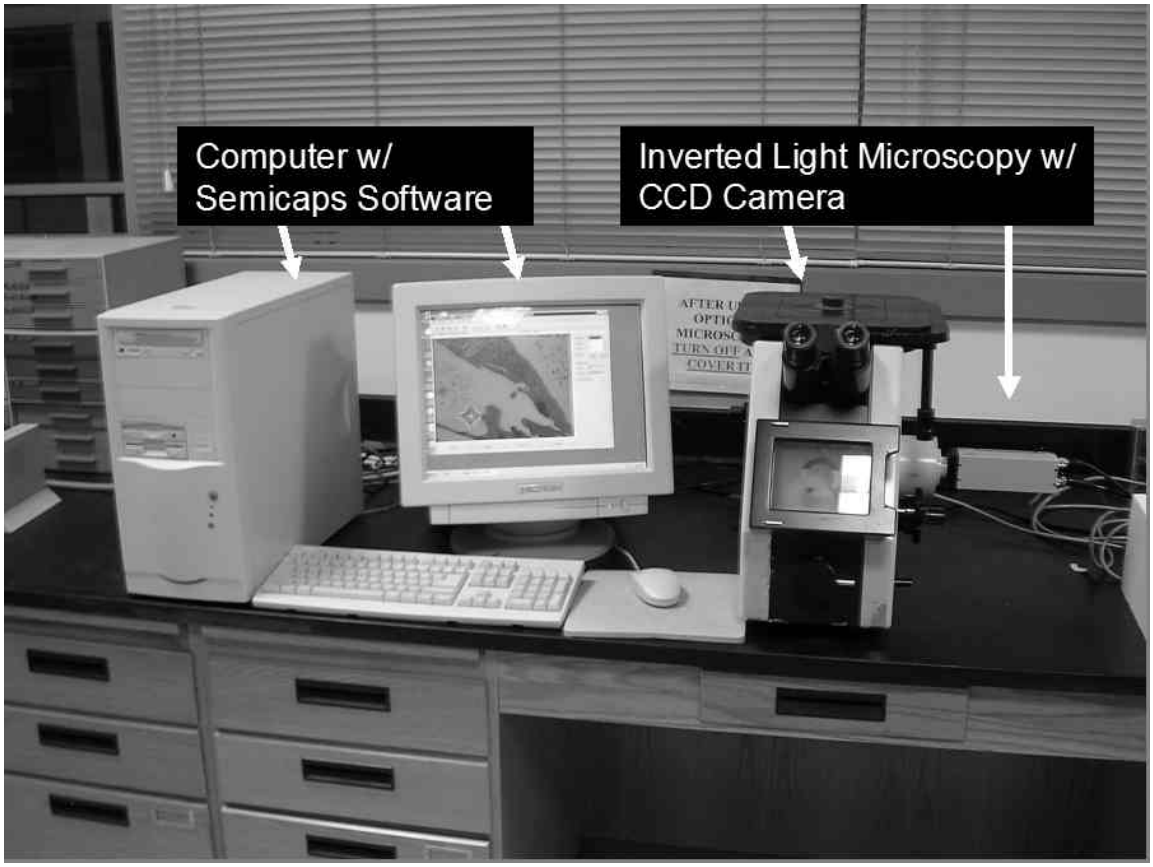

Figure 11. Optical Microscopy Suite

H. MICROHARDNESS TESTING

Microhardness data was collected using a Buehler MICROMET 2004 – microhardness tester fitted with Vickers diamond pyramid indenter (Figure 12). Testing was conducted on all as-cast and treated materials. All hardness measurements were taken with a set dwell time between 10-12 seconds and weight of 100 grams. All indentation diagonal measurements were measured/captured at the highest magnification for the highest accuracy. In all material conditions, measurements were recorded in 20 locations at least 0.005 inches apart to prevent interference from previous indentations. In the cases of rolled material, the twenty measurements were recorded along the ND. Ten additional hardness measurements were also recorded in each of the material conditions to separately capture hardness data for the alpha and beta-prime phases of NAB.

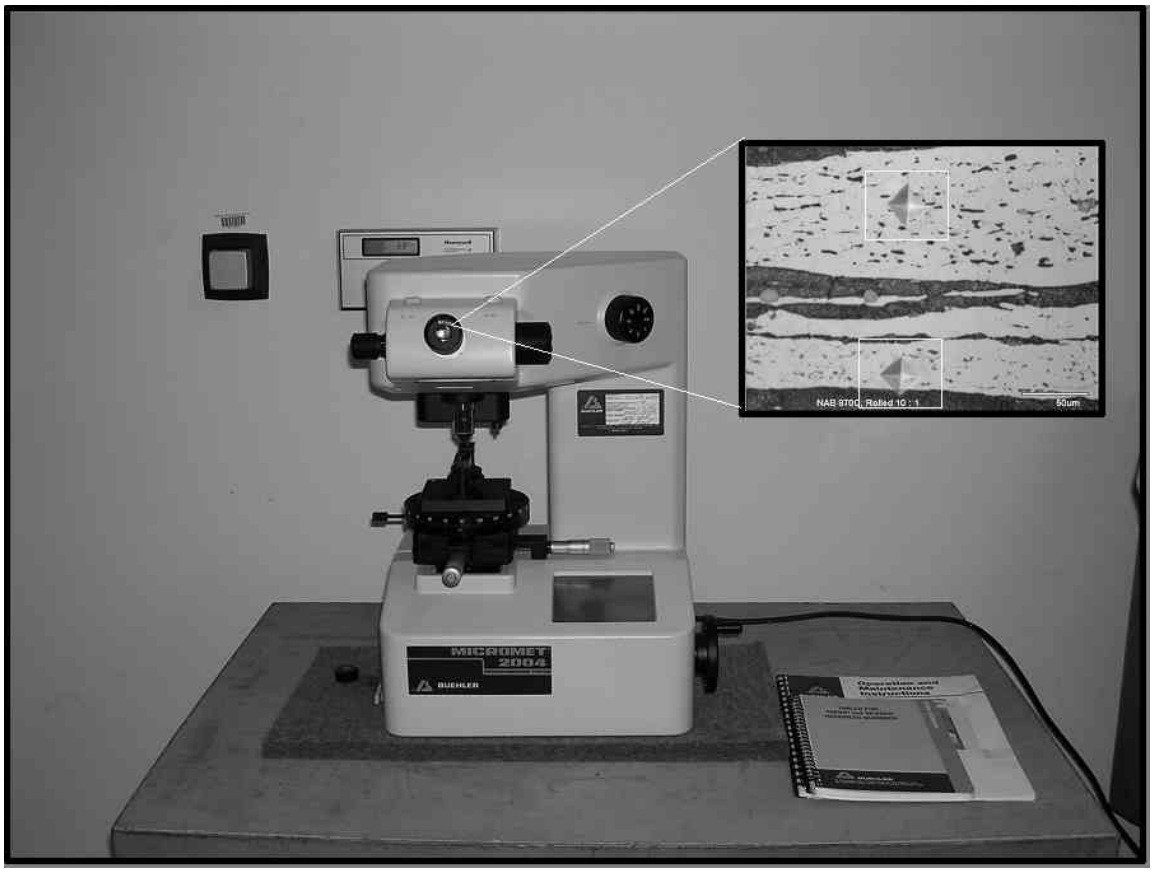

Figure 12. Microhardness Testing Suite

IV. RESULTS AND DISCUSSION

A. ANNEALING AND HOT ROLLING

1. Review: Annealing of Alloy 1

In order to introduce the effect of heating temperature it is useful to review a prior investigation of NAB annealing conducted by Sherburn [Ref. 18]. This study involved isothermal heating and subsequent cooling of as-cast samples heated either for 6 minutes or one hour. The microstructure of the as-cast material is similar to that illustrated for alloy 2 in Appendix A, and consisted of coarse κ_I and κ_{II} particles, coarse primary α containing κ_{IV} precipitates and a eutectoid constituent consisting of lamellar $\alpha + \kappa_{III}$. Samples heated for 6 minutes were water quenched (WQ) , and samples heated for 1 hour were either water quenched or air-cooled (AC). Heating temperatures ranged from 770 – 1000ºC. Micrographs were selected from this work for temperatures similar to those used for hot rolling in the current effort and are presented in Figure 13. Conclusions include the following:

a) Upon heating to 1000ºC for even 6 minutes and rapidly cooling the microstructure consists entirely of β transformation products; the α and κ phases reverted to 100% β upon heating. Water quenching (10^{+3} Cs^{-1}) results in mostly a martensitic β' constituent while slower air cooling (10^{0} Cs^{-1}) results in Widmanstätten α and bainite.

b) At temperatures of 950ºC and below the amounts of the primary α decreased and the amount of β transformation products increased upon increasing heating time from 6 minutes to one hour, suggesting that kinetics for the eutectoid reversion and dissolution of other phases during annealing alone do not give an equilibrium structure in times as short as 6 minutes. It is anticipated that the kinetics of these reactions will be accelerated by concurrent deformation. The incomplete reactions result in retained primary α and, upon cooling of the WQ samples, the formation of martensite, bainite and Widmanstätten α from the β as in the AC samples. The primary α was essentially precipitate free for WQ samples heated above 900ºC. The AC samples show a high density of particles precipitated at α / β interfaces, suggesting a possible source for the nucleation for the α-Widmanstätten from the β.

c) At temperatures of 900ºC and lower the presence of κ phases in both the primary α and β transformation products suggest that these larger κ phases were formed

during slow cooling of the original casting process and did not revert to solution during these annealing treatments. For all κ products in the samples heated for one hour, the microstructures no longer exhibit dendritic features; instead, the particles appear more nearly equiaxed or spherical, suggesting some amount of spheroidizing of these phases.

2. Microscopy of Hot Rolled Material

A matrix of micrographs similar to that of Figure 13 but now for annealed and hot rolled alloy 2 material is shown assembled in Figure 14. The left-hand column of micrographs are for samples that have been annealed only while the center column is for materials rolled to a reduction of 3.5:1 ($\varepsilon_{hotrolled} \approx 1.25$) and the right-hand column are for material hot rolled to a reduction of 10:1 ($\varepsilon_{hotrolled} \approx 2.3$). Each row in Figure 14 is for an isothermal hot-rolling temperature; these samples experienced a total heating time of slightly less than one hour but this can be thought of as reflecting the peak temperature (T_{peak}) of FSP if it is assumed that severe hot deformation accelerates the reversion to the high temperature phases during FSP. Hot rolled sheet material was allowed to air cool at the completion of rolling and it is anticipated that such cooling takes place at a rate similar to that encountered during FSP. The most significant feature of the resulting micrographs is the respective volume fractions of primary α and β transformation products. A summary of volume fraction measures for these constituents is presented in Figure 15; the κ phases were lumped with the primary-α due to the relatively small fraction these other products (~ 0 - 2%). For alloy 2 (Table 2) a significant fraction of the alloy remained primary α upon heating to 1000ºC. The volume fraction of primary α was measured to be 25% in annealed material. This differed from the result for Alloy 1, which had reverted completely to β upon heating at the 1000ºC temperature. Over the entire temperature range of this investigation the apparent volume fraction of primary α was higher and the volume fraction of β transformation products was lower than in Alloy 1. These differences are attributed to their differing compositions, wherein Alloy 2 is higher in Al, Ni and Fe concentrations. From the schematic phase diagram reported by Brezina for NAB (Figure 16) one might expect that an increase in Al content will result in an increase of β transformation products but this is not the case here. It is noted that both annealed and hot rolled materials gave similar results so that it is unlikely that the

deformation and temperature cycling associated with hot rolling lead to a change in volume fraction of β transformation products. It is deem most likely that the increased Ni and Fe concentrations have a greater effect than the increase in Al content when Alloy 2 is compared to Alloy 1. Thus, the increased Ni and Fe concentrations would increase the amount of Al tied up in the various κ phases and the net result would be that the phase boundary between the β region and the $\alpha + \beta$ two phase region suggested by Brezina [Ref. 14] is further to the right for 9.8% Al; this is indicated in Figure 16.

3. Correlation of Microstructures in Hot Rolling and FSP

Microscopy results from a transverse section of single-pass FSP material are shown in Figure 17. This matrix of microstructure results for deformed materials and sections from this study were place side by side for the sake of facilitating comparison. These data shows stir zone (SZ) microstructures and hot rolled materials at two different magnifications for each. It is apparent for the FSP material that different regions under go different strains and reach different peak temperatures. Distinct boundaries of regions can be resolved from the variations in degree of grain refinement, relative phase volume fractions and flow patterns within the SZ. Features include bands, lamellar structures, and onion ring patterns. The Widmanstätten α is apparent at many locations suggesting that heating temperatures have been sufficient to form β during FSP. Understanding the parameters required for the formation of these structures from a cast condition will enable the correct interpretation of the strain and temperature history within the FSP region. For example, the lamellar structure formed in region 2 of the FSP material (Figure 17) compares well with the lamellar structure for material hot rolled at 950ºC. From this, it can be concluded that the local peak temperature, T_{peak}, at region 2 was also ~950ºC. Quantitative evaluation of the amount of β transformation products (darker etched regions) in conjunction with the type of product formed (Widmanstätten α, bainite or martensitic β') will enable more refined estimates for the T_{peak} and cooling rates observed.

4. Microscopy Data

Micrographs for all conditions have been included in Appendix A. Selected conditions will be included in this section.

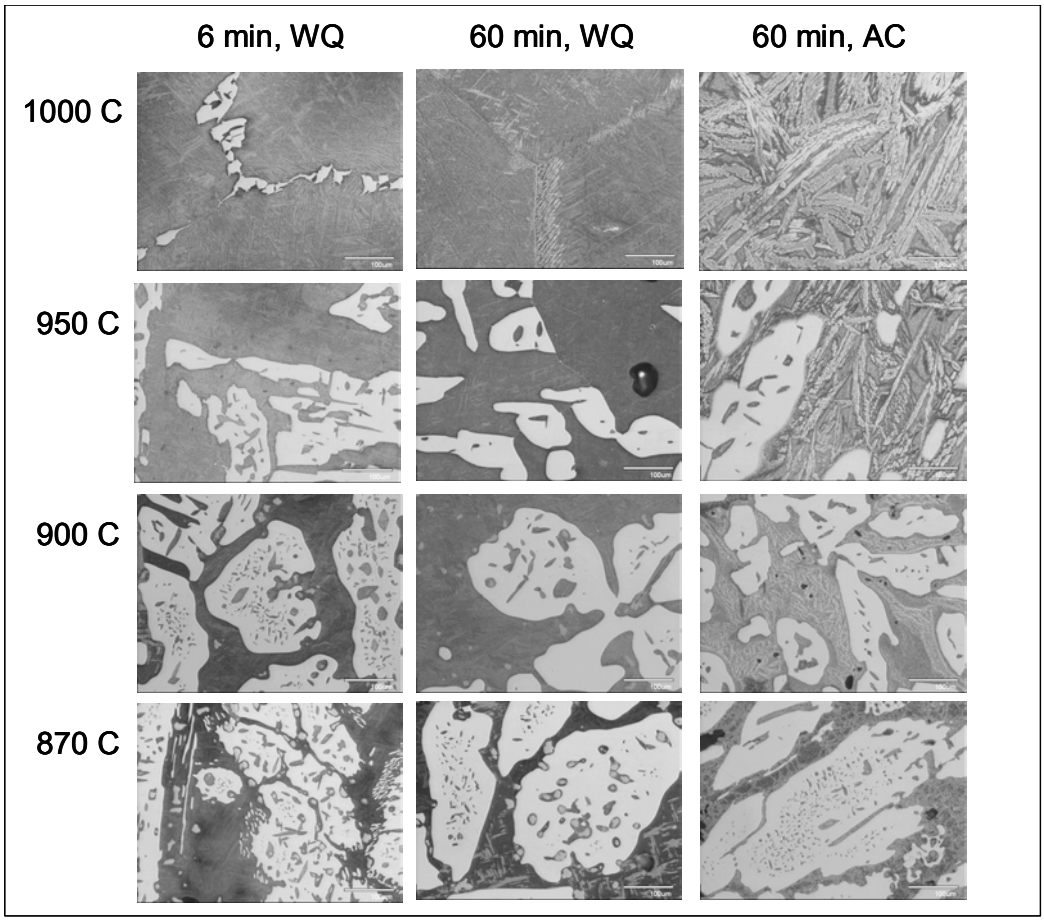

Figure 13. NAB Isothermal Annealing Study – (micrographs courtesy of J. Sherburn, NPS)

Optical micrographs are magnified 370x. Micron markers represent 100 μm. Alloy composition is that of Alloy 1 from Table 2. Lighter regions are α, darker represents β. All times represent length of isothermal heat treatment, WQ – Water Quenched; AC – Air-Cooled.

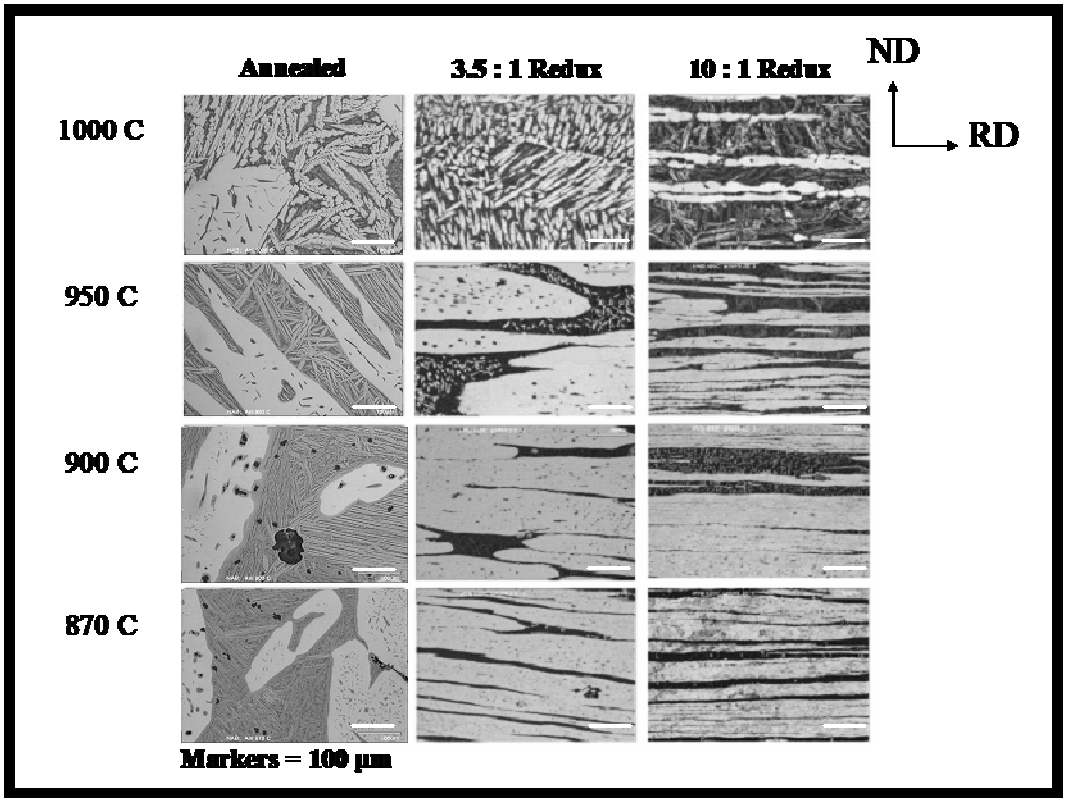

Figure 14. NAB Isothermal Anneal and Hot-Rolling Study (Alloy 2)

Optical micrographs magnified 370x. Micron markers represent 100 μm. Alloy composition is that of Alloy 2 from Table 2. Lighter regions are α, darker represents β.

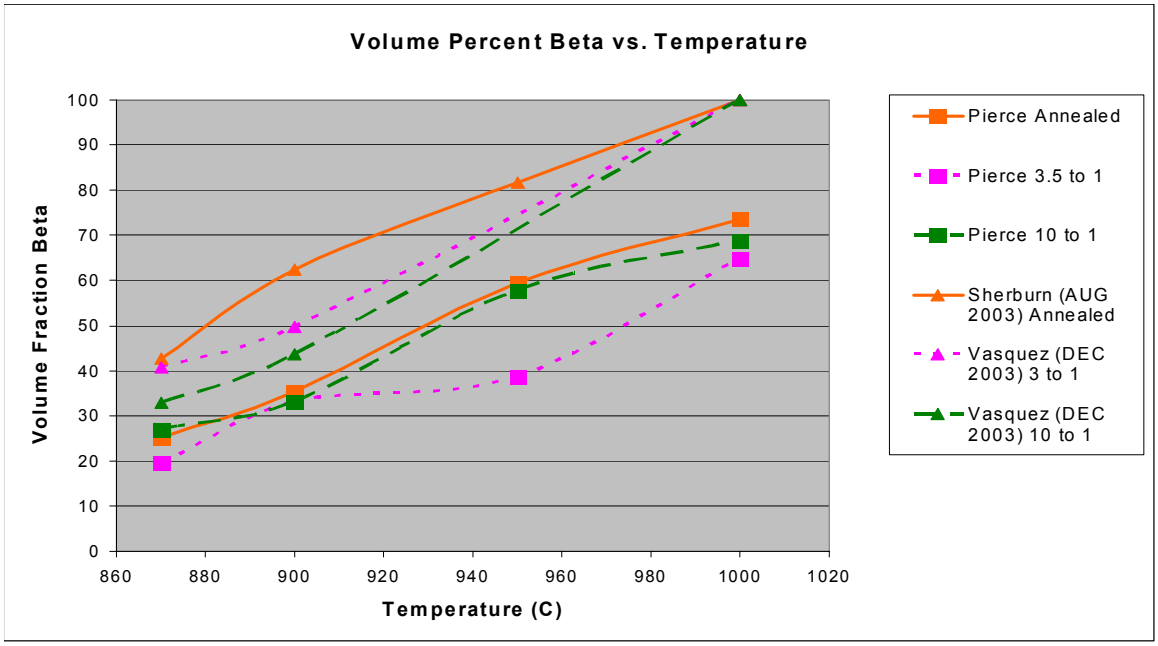

Figure 15. Volume of β (%) vs. Process Temperature

The graph displays results of measurements taken from micrographs using pixel counts for alpha and beta regions. Regions defined and verified by hand using a computer brush. Micrographs were forced to 8 colors, no pattern, diffusion or dithering this allows for the steepest gradient between colors. Lighter regions were considered alpha, darker represented beta. Fractions were obtained from percentage of overall pixel count.

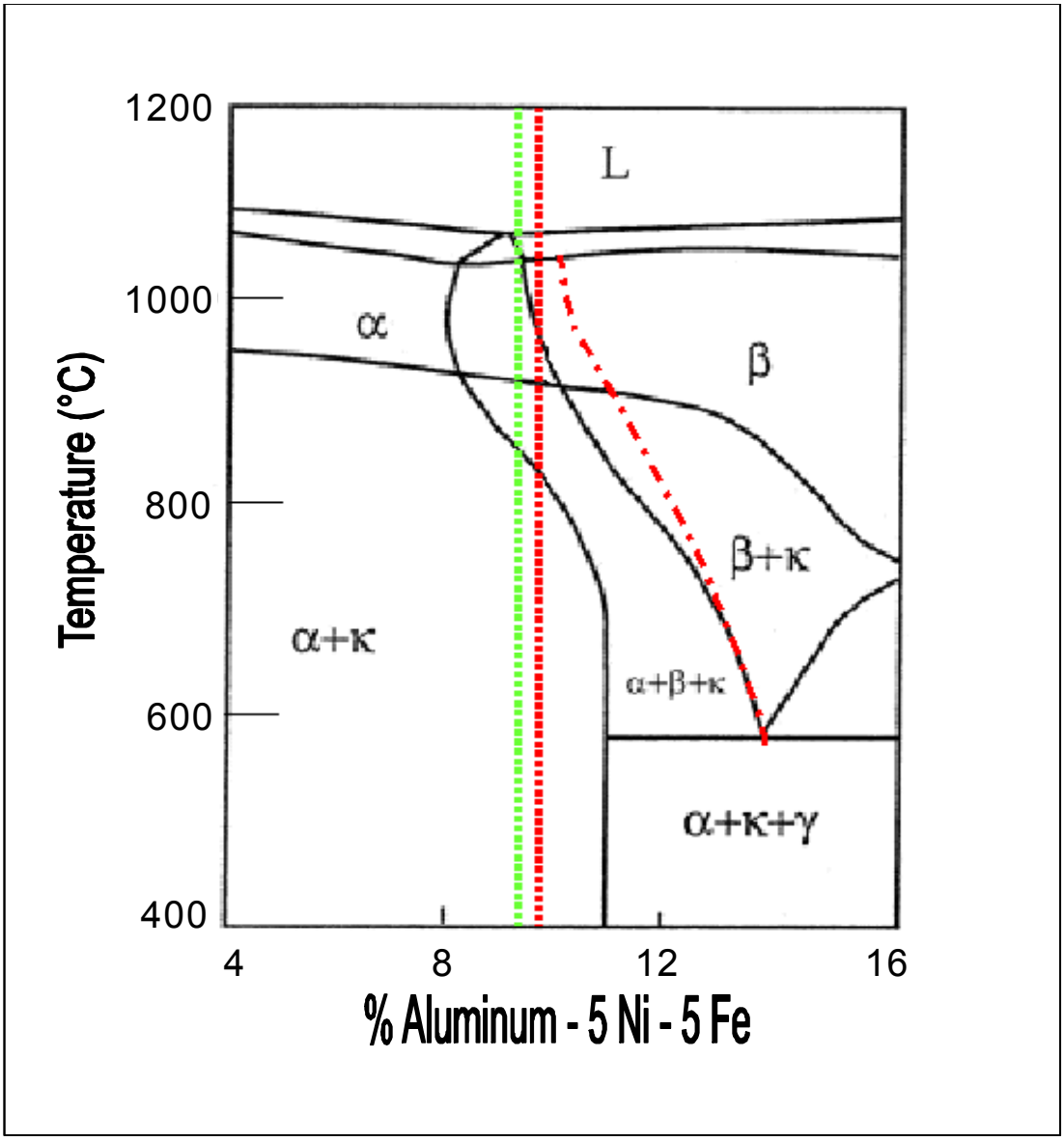

Figure 16. Vertical Section of the Cu – Al – 5 Ni – 5 Fe Equilibrium Diagram (adapted from Ref. 14)

Phase schematic adapted from Brezina. Note that the vertical dotted lines represent the percentage of Al for Alloy 1 (9.4%) and Alloy 2 (9.8%) respectively, also the dot-dashed line has been drawn to reflect the measured amounts of α and β in Alloy 2 (Cu – 9.8 Al – 4.71 Ni – 4.95 Fe).

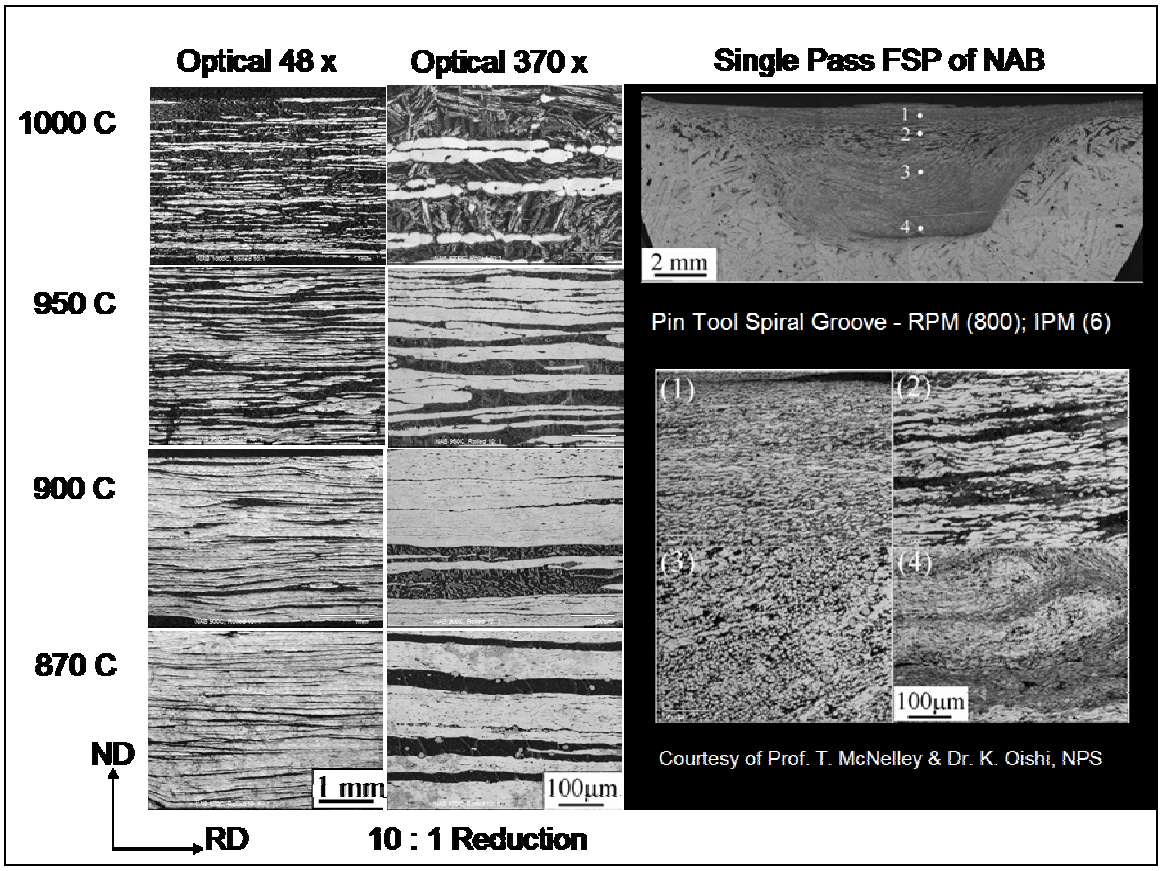

Figure 17. Microscopy Comparison Hot-Rolled vs. Single Pass FSP

Optical micrographs show comparison between FSP and hot-rolled material. Micron markers altered only for contrast. Alloy composition is that of Alloy 2 from Table 2. Lighter regions are α, darker represents β. FSP material is closer to that of Alloy 1. FSP transverse section is shown with retreating side on the left and advancing side on the right. Micrographs for regions in stir zone are magnified 370x.

B. MECHANICAL TEST RESULTS

1. Hardness Data

In previous work a microhardness survey was completed through a transverse section of FSP material. The Vickers hardness values measured for the SZ, TMAZ and base metal are summarized in Figure 18. The hardness obtained in FSP material is significantly greater than the surrounding base metal and there is a steep gradient in hardness near the base metal – TMAZ boundary. The transition from base metal values

of HV150 to HV250 in the SZ occurs within 1 mm. Another feature the data is consistent hardness throughout the SZ. This would suggest a relatively uniform distribution of prior strains, temperatures and microstructures in the material; however microscopy results very different and distinct microstructural regions.

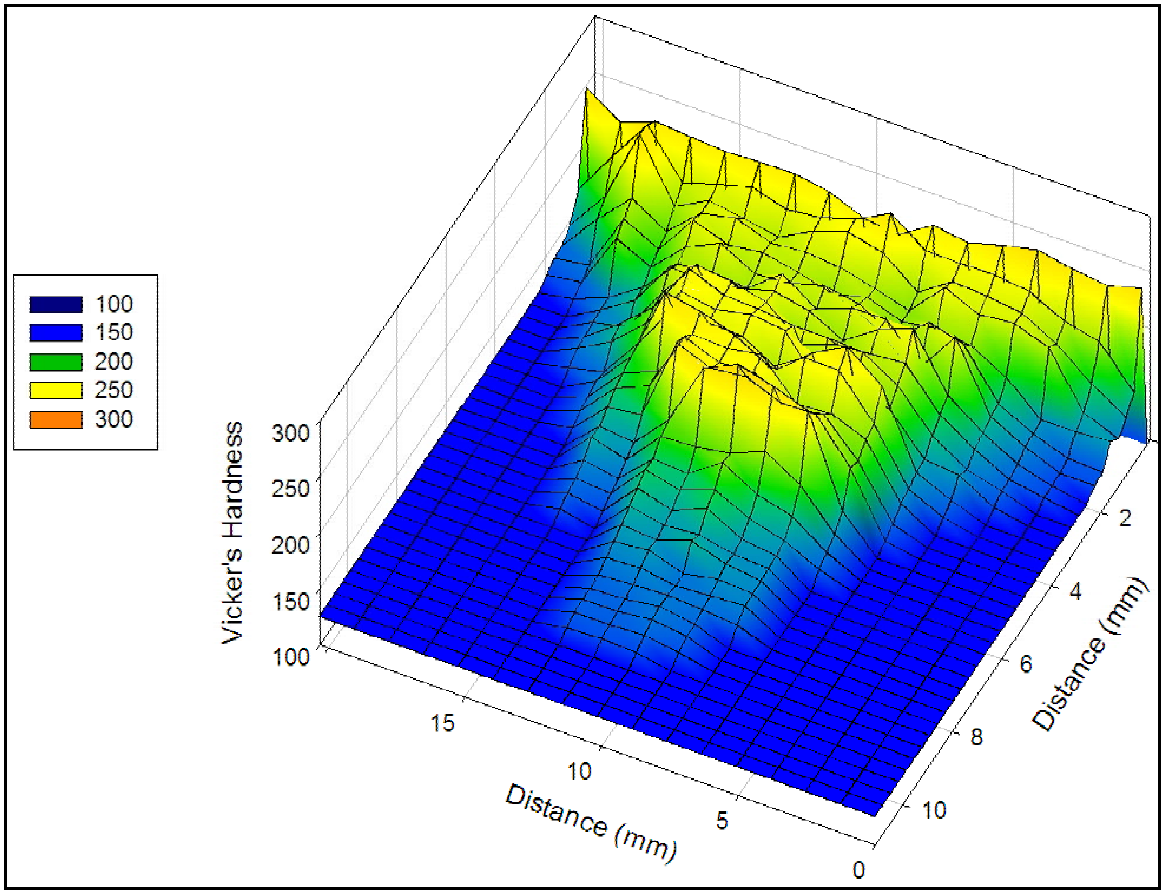

Figure 18. Vickers Hardness Survey – FSP 516 (courtesy of Dr. C. Park, NPS)

Microhardness data for all hot rolled conditions were obtained and are shown in Figures 19 and 20. Figure 19 represents the average Vickers hardness recorded in the processed material. These data suggest that the hardness is independent of hot rolling temperature, which is a very surprising result. Increased rates of recovery during deformation at higher temperatures would be expected to give a decreasing hardness as hot rolling temperature increases. Nevertheless, this is consistent with the high and relatively flat distribution of hardness in the stir zone of one material despite

microstructural evidence of varying peak temperatures. Subsequently, microhardness measurements were made separately on primary α and the β transformation products and the results are summarized Figure 20. Here, the hardness of both microstructure constituents decreases with increasing hot rolling (or annealing) temperature; nevertheless, the hardness of the β transformation products is always greater than that of the primary α. It can be surmised that the increased volume fraction of β transformation products upon increasing the hot rolling temperature (or in regions of high T_{peak} in the SZ) offset the effects of enhanced recovery rates expected in locations of high local temperature. This is apparent in macrohardness data as indicated in Figure 21 for both annealed and hot rolled materials. Heat treatment alone resulted in increased hardness with increasing temperature, mainly because of the increased amount of β present. The average hardness values measured for the deformation processes varied by as much as 10 points of the Rockwell B-scale but tended to be higher at lower deformation temperatures and this may be a result of the competing effects of strain hardening and high temperature softening.

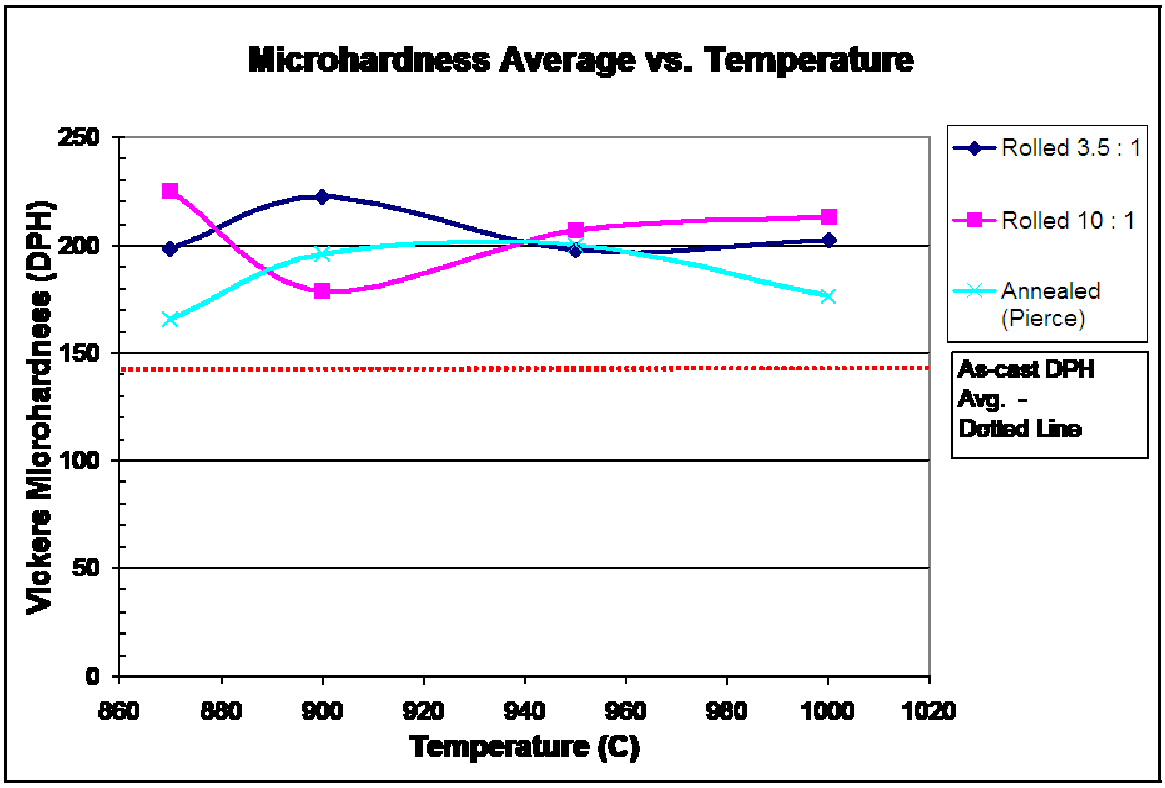

Figure 19. Microhardness Test Results – Average Hardness vs. Process Temperature

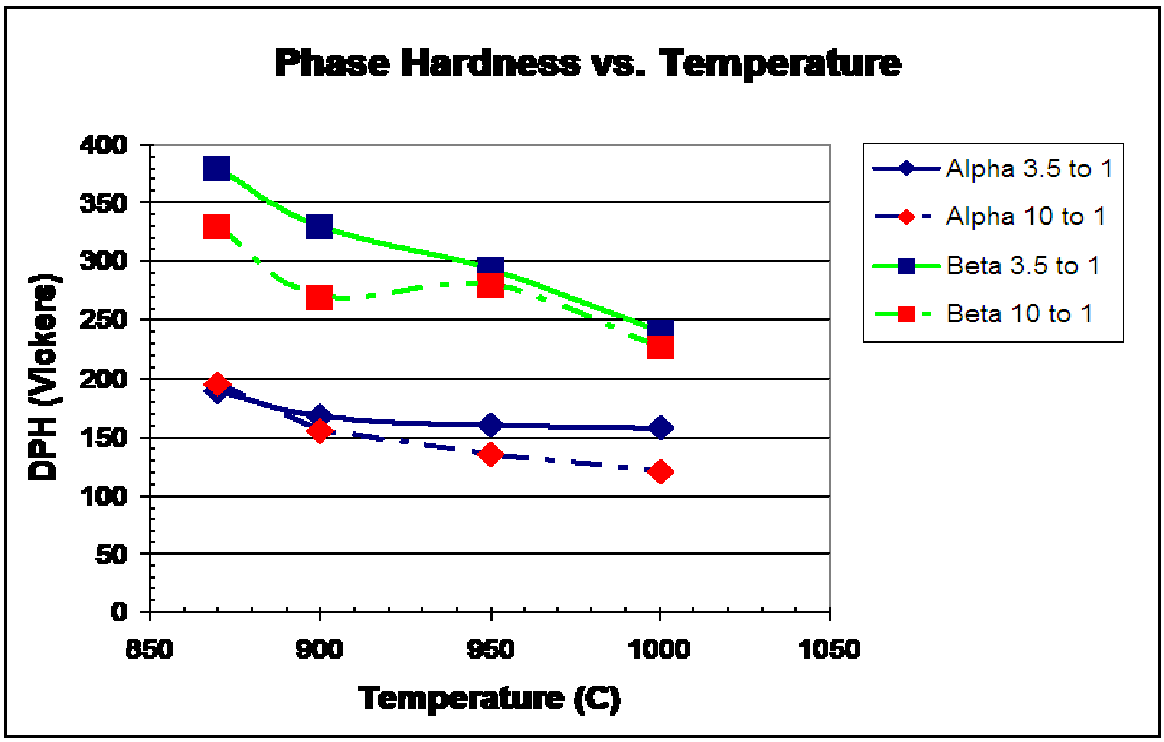

Figure 20. Microhardness Test Results – Phase Hardness vs. Temperature

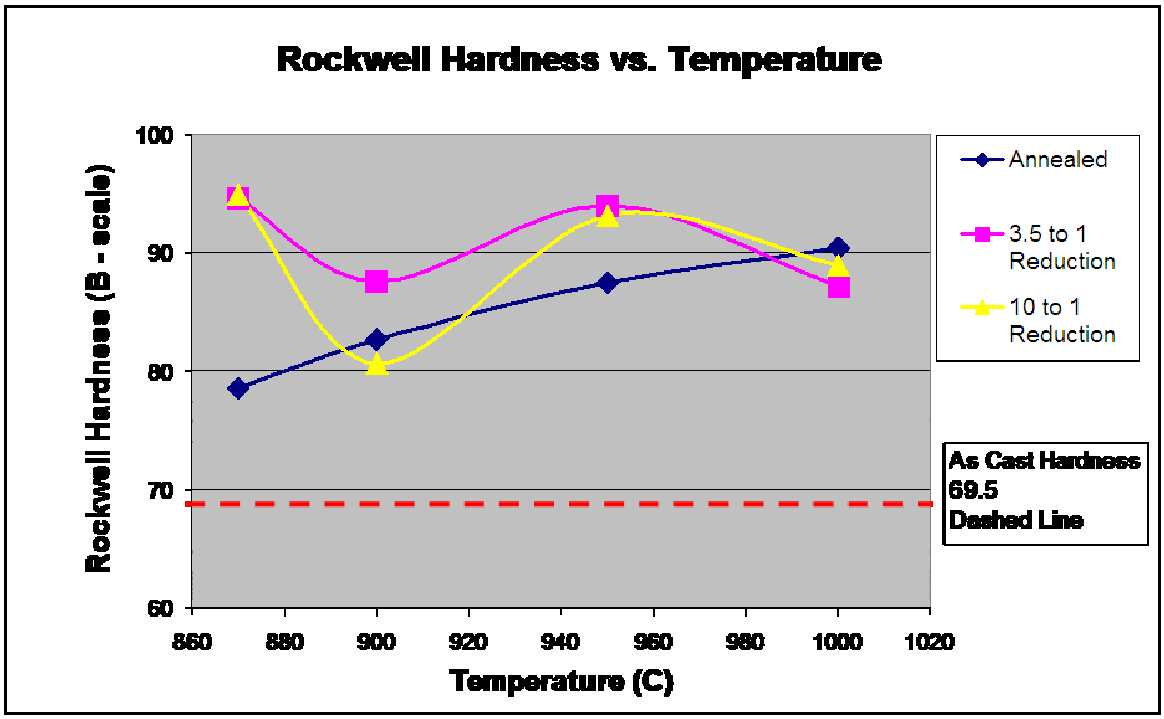

Figure 21. Macrohardness Test Results – Rockwell Hardness vs. Temperature

2. Tensile Testing Results

Tensile testing was used to determine the mechanical properties associated with the as-cast, annealed and hot rolled materials. The data of this testing is summarized in Figure 22 for the ultimate and yield strengths (UTS, YS) measured for the conditions as indicated. All values exceed those measured for the as-cast condition. Overall, annealing alone of the as-cast material for one hour at temperatures between 870 – 1000ºC improved YS and UTS by 20-30 percent over the as-cast condition while strength increases for the hot-rolled conditions varied from 185-225%. General trends to be noted for the hot-rolled materials are that increased hot rolling temperatures result in a slight decrease for both YS and UTS values upon increasing the hot rolling temperature from 870 to 900ºC. In material hot rolled to a 3.5:1 reduction the yield strength decreases further at higher hot rolling temperatures while the UTS increases at higher hot rolling temperatures. The material hot rolled to a 10:1 reduction exhibits a flat YS with increasing hot rolling temperature and a significant increase in UTS as hot rolling temperature increases from 900 to 1000ºC.

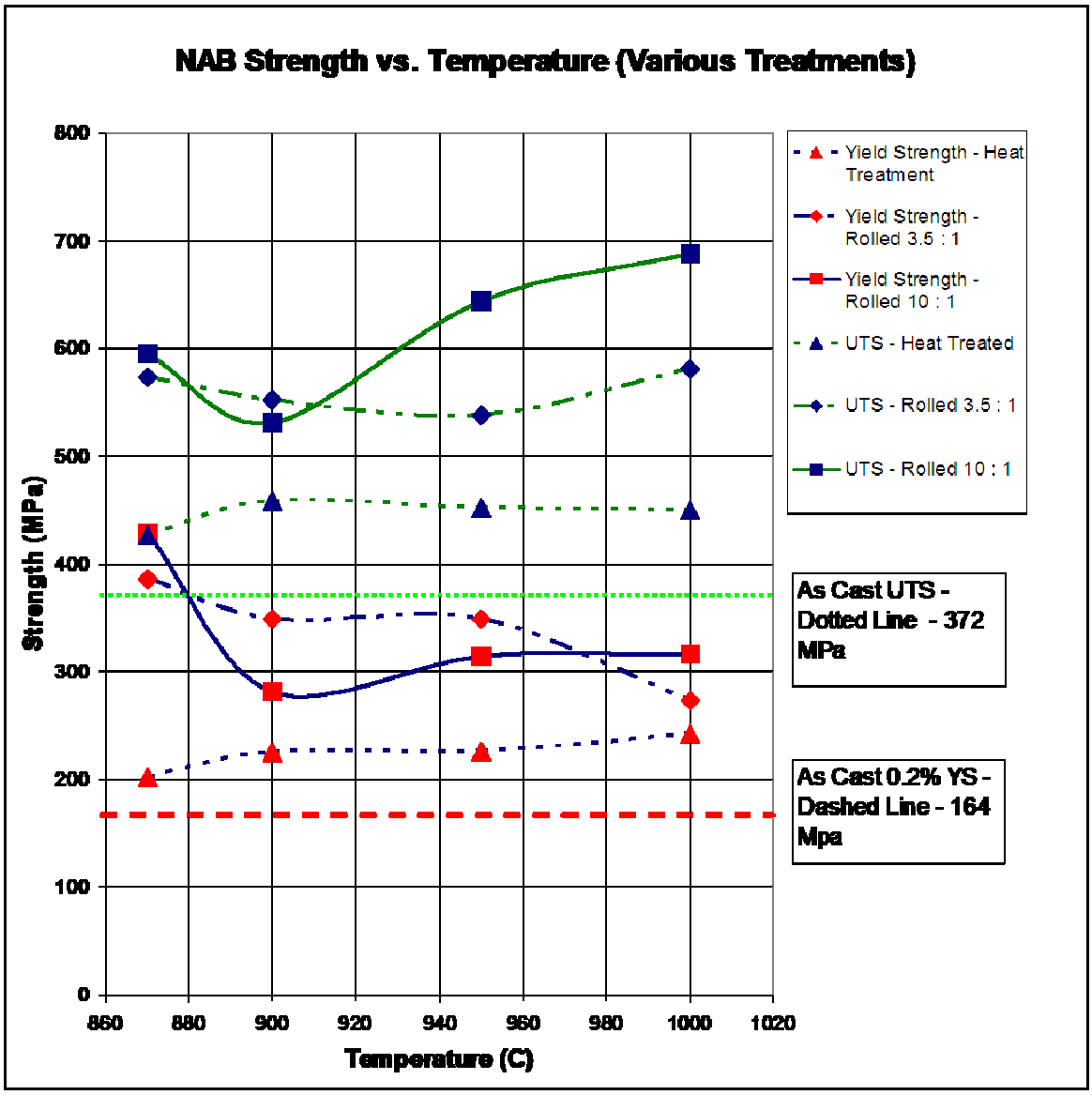

Figure 22. Tensile Test Results – Strength vs. Temperature

Plot generated from tensile data averaged from more than 120 tensile tests, each point represents as sample set of no less than four. Statistical outliers were removed and tests re-run. All tests were run at ambient temperature.

Corresponding ductility values are against hot rolling temperature as shown in Figure 23. The average ductility for the as-cast material was ~11%, although it should be noted that the standard error was large (6.5 %) even after removal of invalid samples from the data set. The lowest measured ductility value for as-cast material was 4.5% and largest was 23%. All tests conducted for the various annealing and hot rolling conditions exhibited noticeably more consistency. Ductility values for the sample set representing

the material rolled with a 3.5:1 reduction at 950ºC appears low although a review of the samples and test set-up offered no reasons to invalidate any of the measured results.

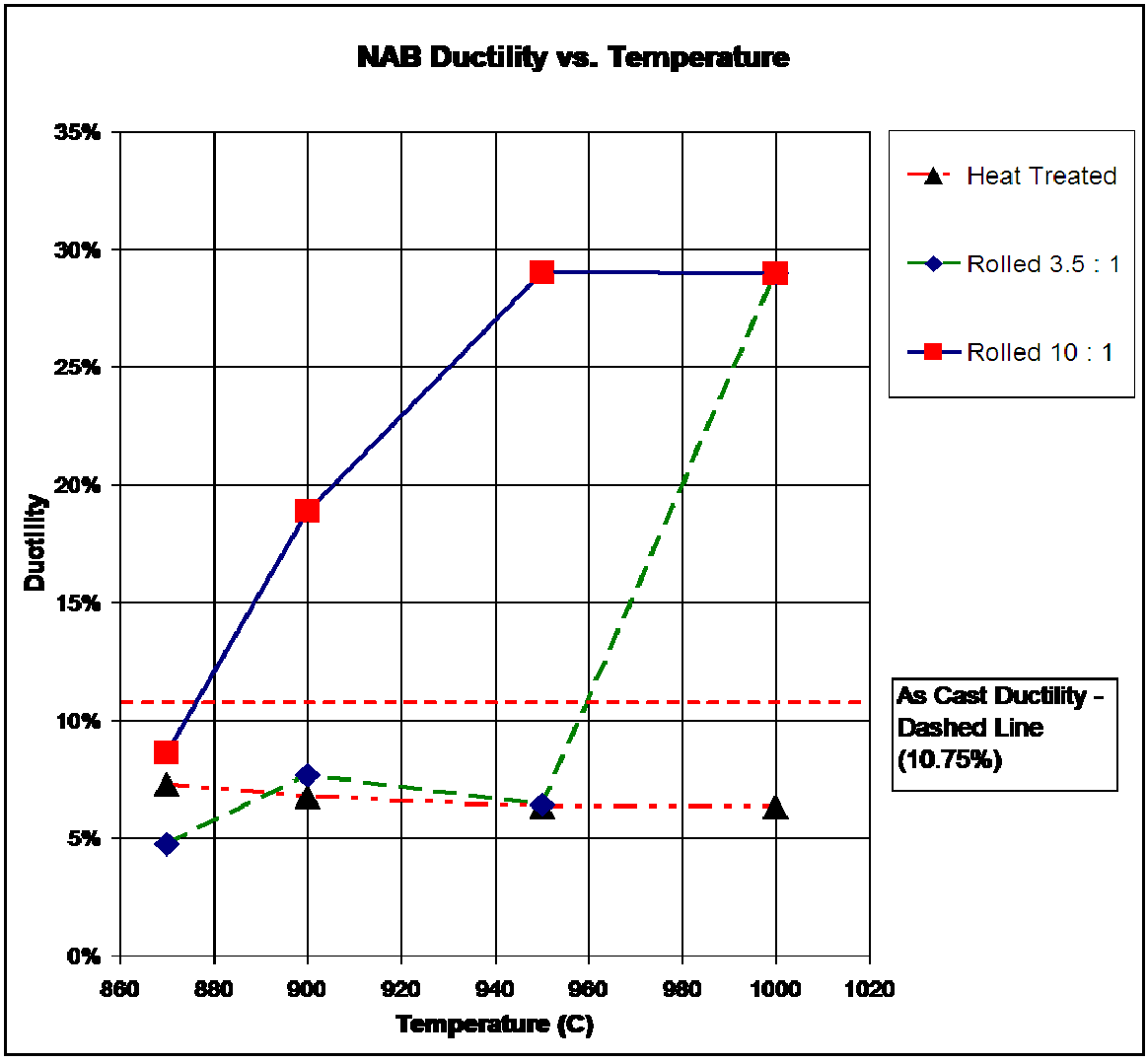

Figure 23. Tensile Test Results - Ductility vs. Temperature

Plot generated from tensile data averaged from more than 120 tensile tests, each point represents as sample set of no less than four. Statistical outliers were removed and tests re-run. All tests were run at ambient temperature.

As a potential surface hardening treatment for components fabricated from as-cast NAB the increased values of YS, UTS and ductility due to FSP are highly desirable. Especially noteworthy are the results for materials hot rolled to a 10:1 reduction at temperatures of 950 - 1000ºC. These data suggest that FSP of materials under conditions

leading to peak temperatures in this range will result in high strength due to a high fraction of β transformation products coupled with a high (28% elongation). It should be noted that the microstructure of the material of this study, Alloy 2, still includes primary α as well as β transformation products characteristic of air cooling of the material after hot rolling. These products are predominantly Widmanstätten α and bainite. Nevertheless, these results suggest combinations of high RPM and low IPM, resulting in high peak temperatures, will provide good combinations of strength and ductility.

3. Mechanical Testing Data

Tabular data for the information presented have been included in Appendix B.

THIS PAGE INTENTIONALLY LEFT BLANK

V. SUMMARY AND CONCLUSIONS

Based on the results of this study of microstructure and material properties, and of the relationships between isothermal hotworking and the FSP process, the following conclusions are drawn:

1. Isothermal hotworking of NAB provides high ductility with little loss of yield and tensile strength for hot rolling temperatures of 950 - 1000ºC. Increased rolling strain at the highest temperatures enhanced both the YS and UTS while providing the largest values of ductility. For a single FSP pass this correlates to tool parameters of high RPM coupled with low IPM.

2. Hardness distributions for single-pass FSP and for isothermal hotworking of NAB material are relatively flat with increasing temperature despite the variations in corresponding microstructures. This is a result of increased volume fractions of β transformation products, which are harder than the primary α, upon heating to higher temperatures in the regime above the eutectoid at 800ºC. This is apparent in both hot rolled and FSP material.

3. Microscopy analysis confirms the capability to predict T_{peak} in FSP material in regions exhibiting lamellar structures. The separate temperature and deformation processes consider in this experiment did not clarify processes involved in other regions, including banded, onion ring and spheroidized particles.

4. Microscopy highlighted the importance of alloy composition when interpreting mechanical and microstructural analysis. Results of this research were influenced by increased amounts of Fe and Ni.

Research into the behavior of NAB material at isothermal definitions has provided definitive insight into certain regions especially the flow arm and lamellar regions of the FSP stir zone. Different testing parameters will be required to form the other resultant microstructures including the banded, onion ring and spheroidized regions. Future work to include characterization of stir zones in multi-pass and raster FSP may result in yet different microstructural regions and their properties.

THIS PAGE INTENTIONALLY LEFT BLANK

APPENDIX A - MICROGRAPHS

A. AS-CAST

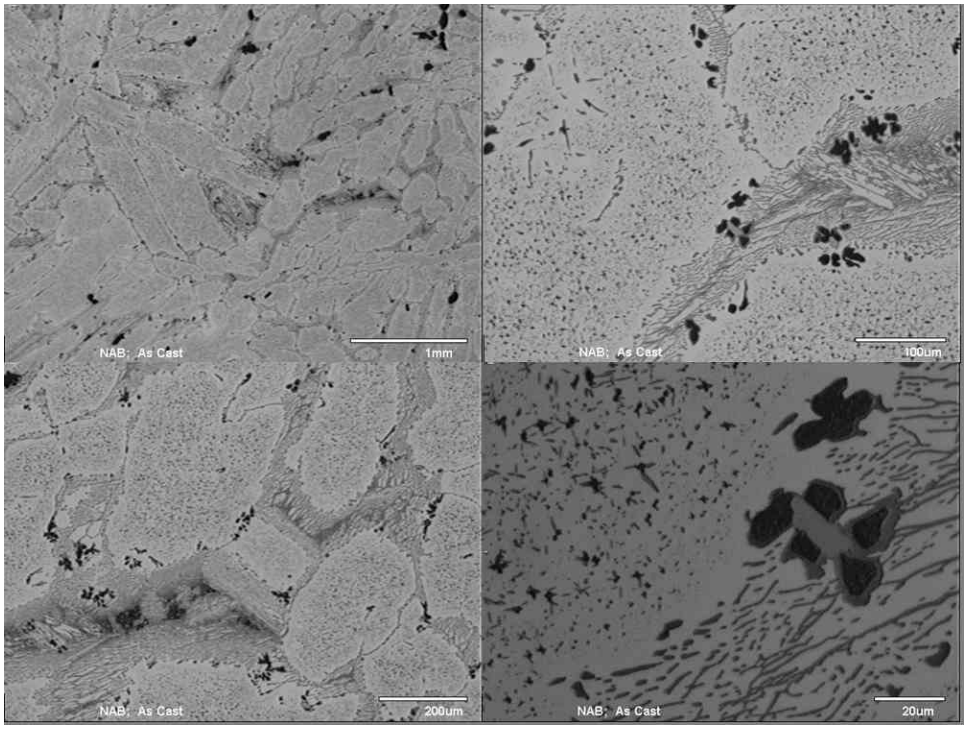

B. ANNEALED 870 C – AIR-COOLED

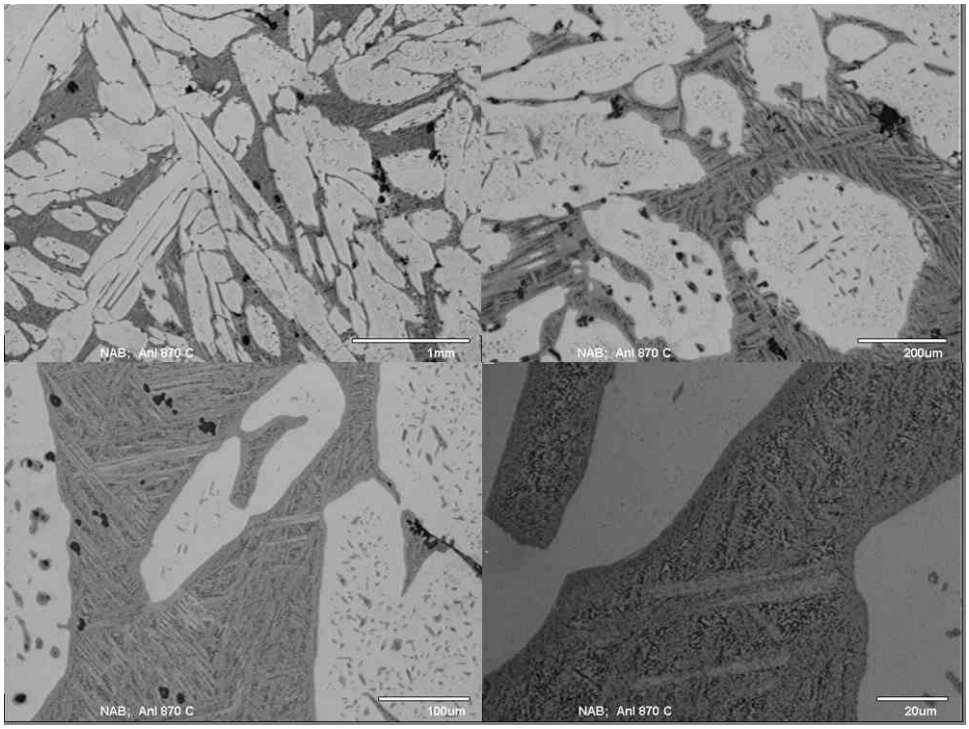

C. ANNEALED 900 C – AIR COOLED

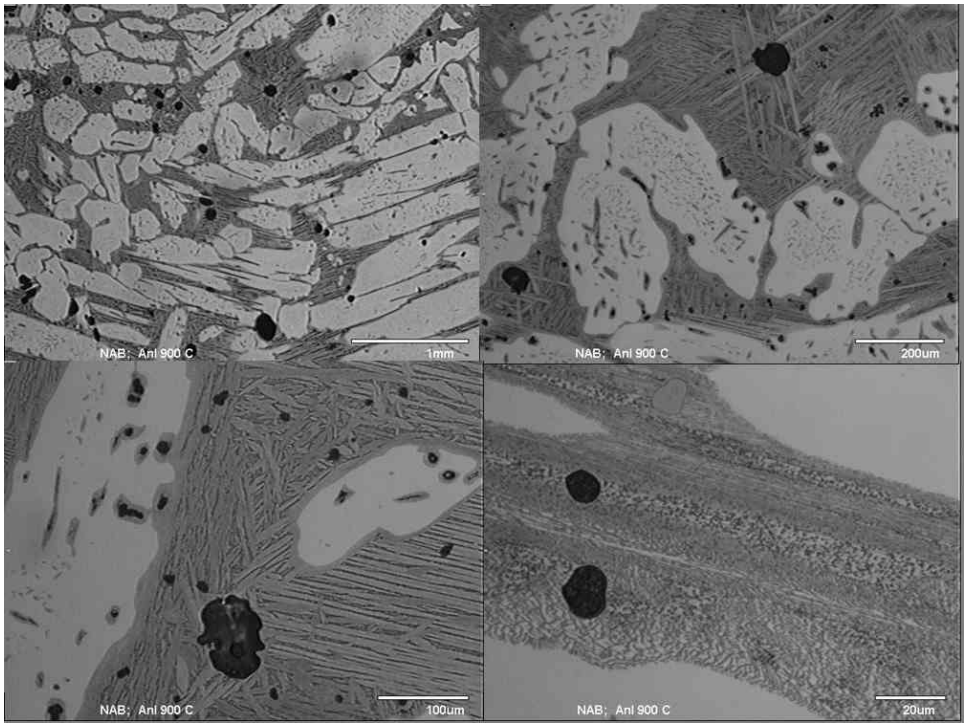

D. ANNEALED 950 C – AIR COOLED

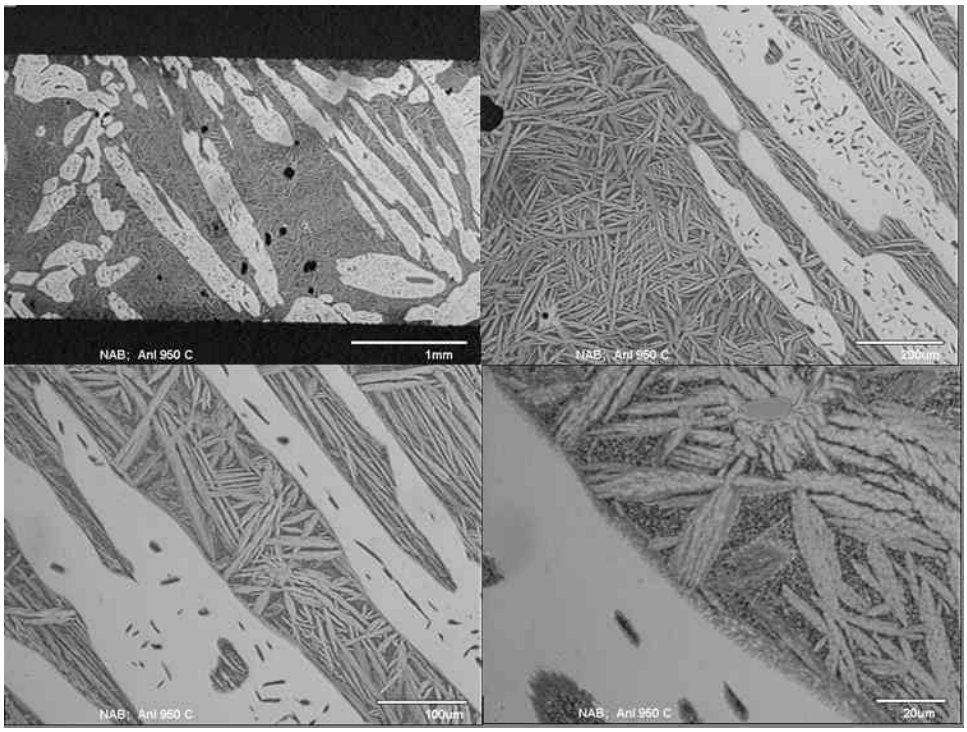

E. ANNEALED 1000 C – AIR COOLED

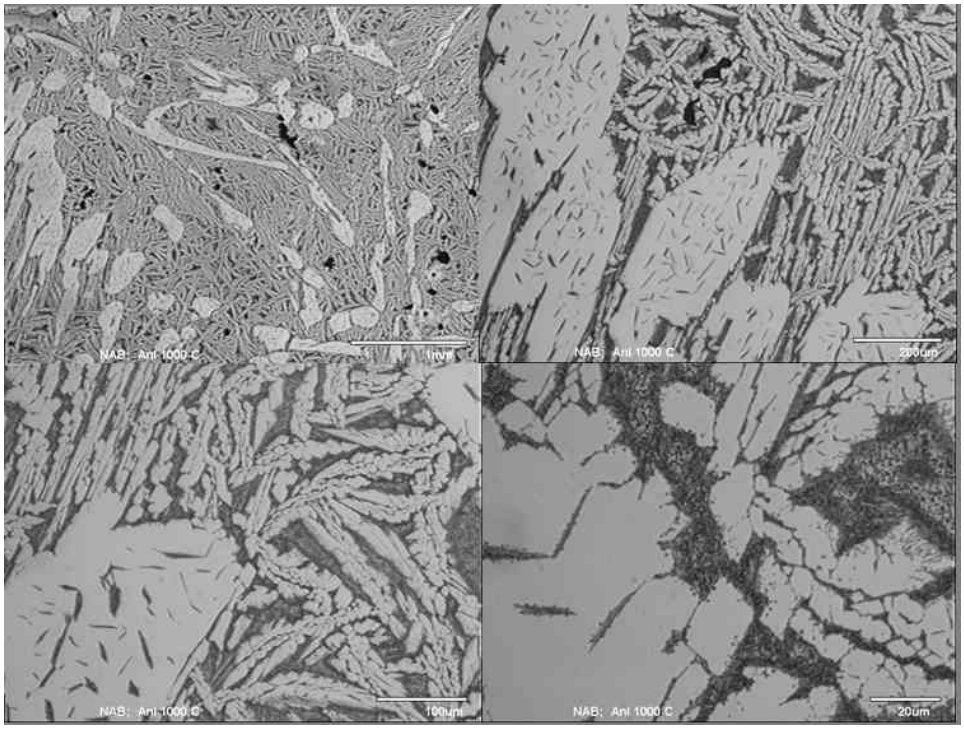

F. ROLLED 3.5 : REDUCTION, 870 C – AIR COOLED

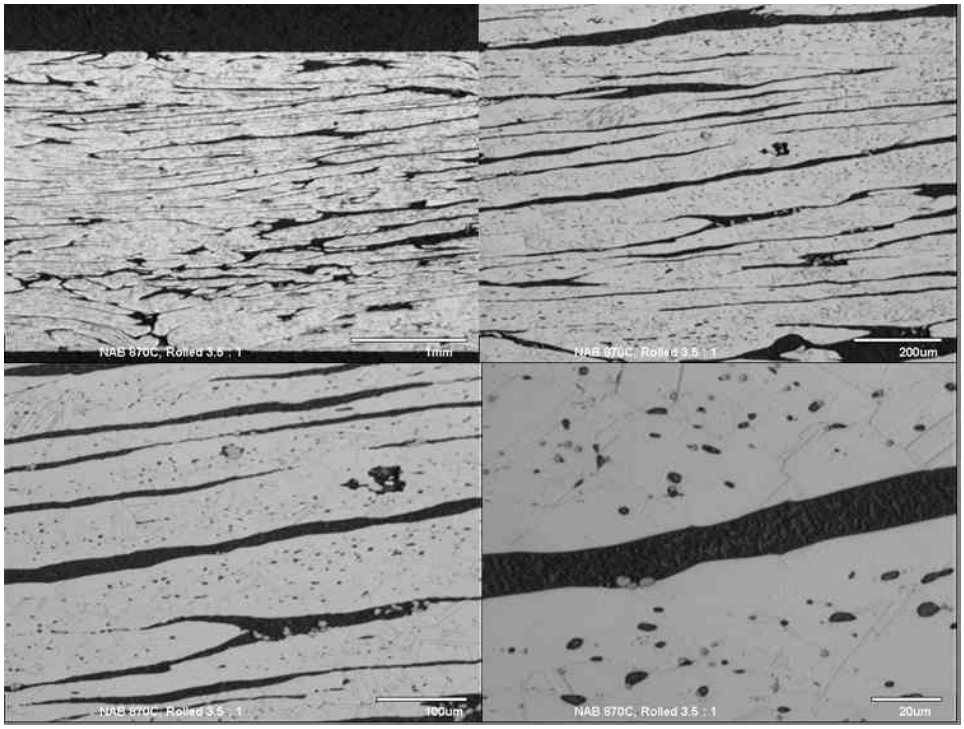

G. ROLLED 3.5 : 1 REDUCTION, 900 C – AIR COOLED

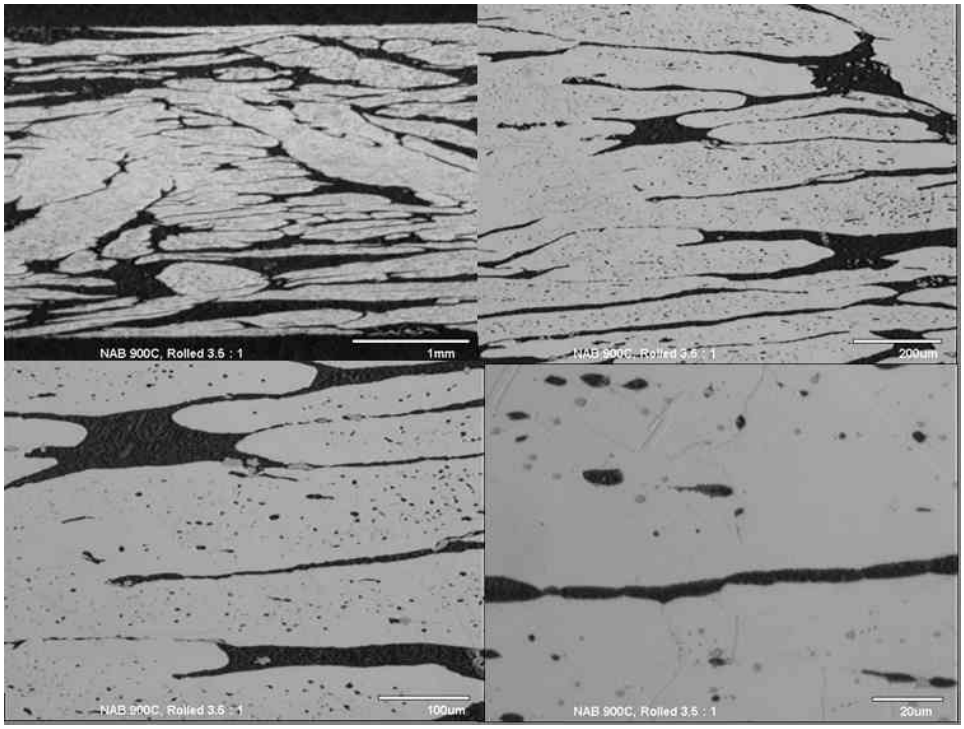

H. ROLLED 3.5 : 1 REDUCTION, 950 C – AIR COOLED

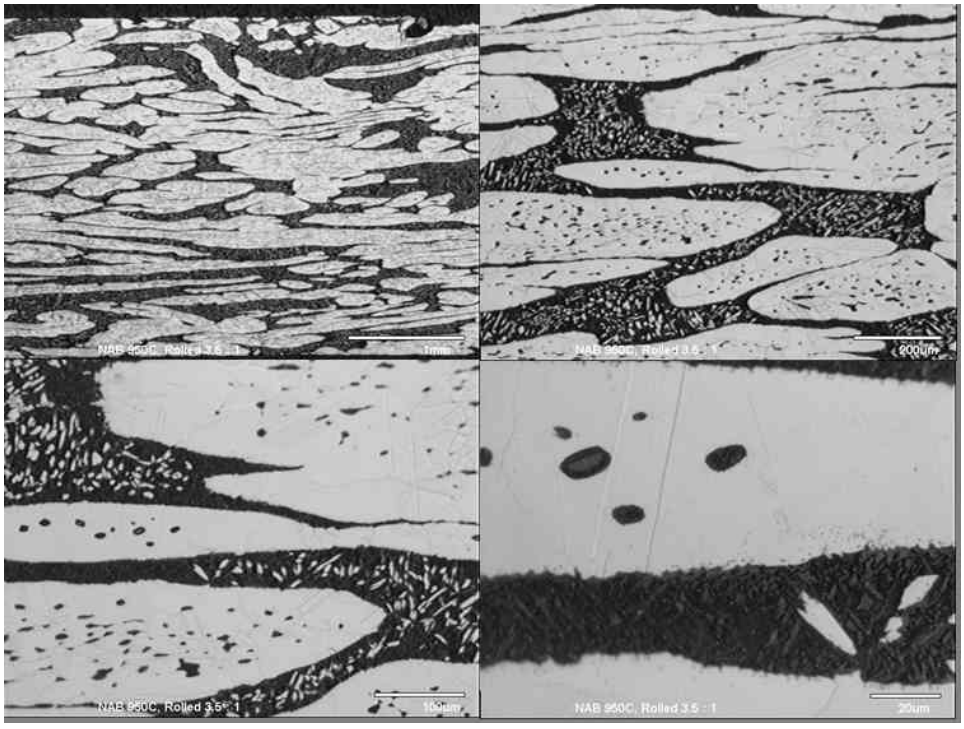

I. ROLLED 3.5 : 1 REDUCTION, 1000 C – AIR COOLED

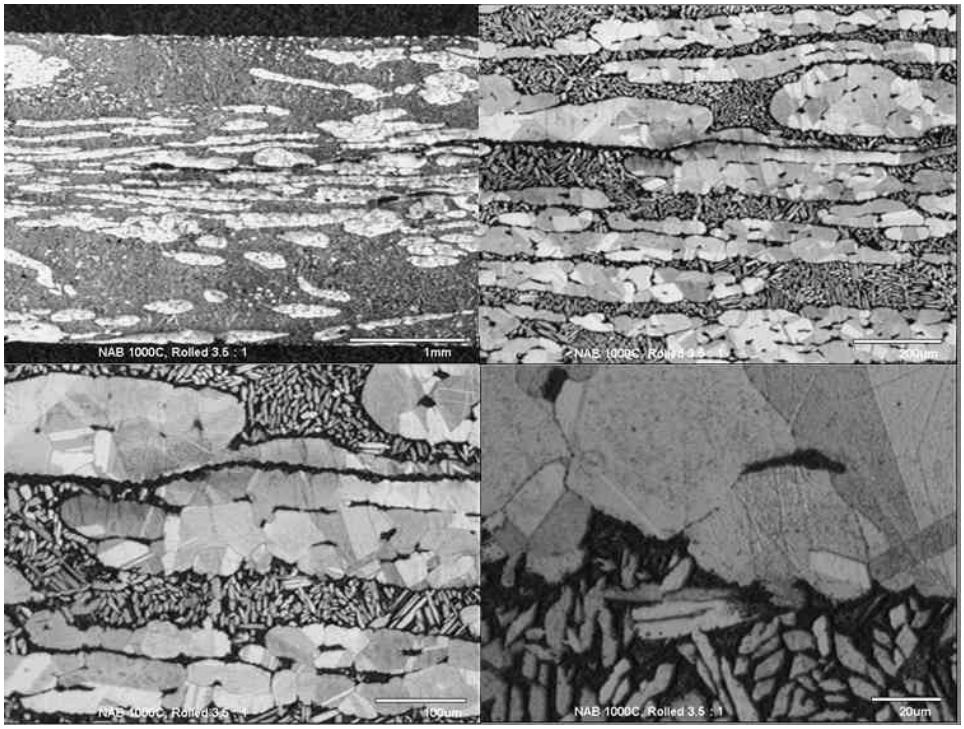

J. ROLLED 10 : 1 REDUCTION, 870 C – AIR COOLED

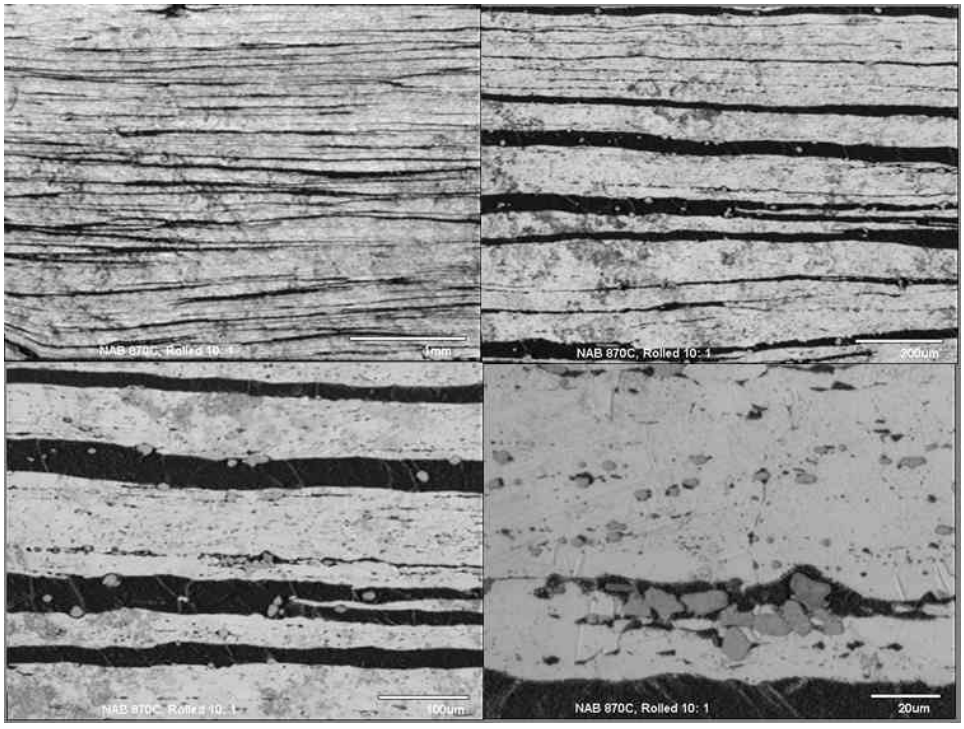

K. ROLLED 10 : 1 REDUCTION, 900 C – AIR COOLED

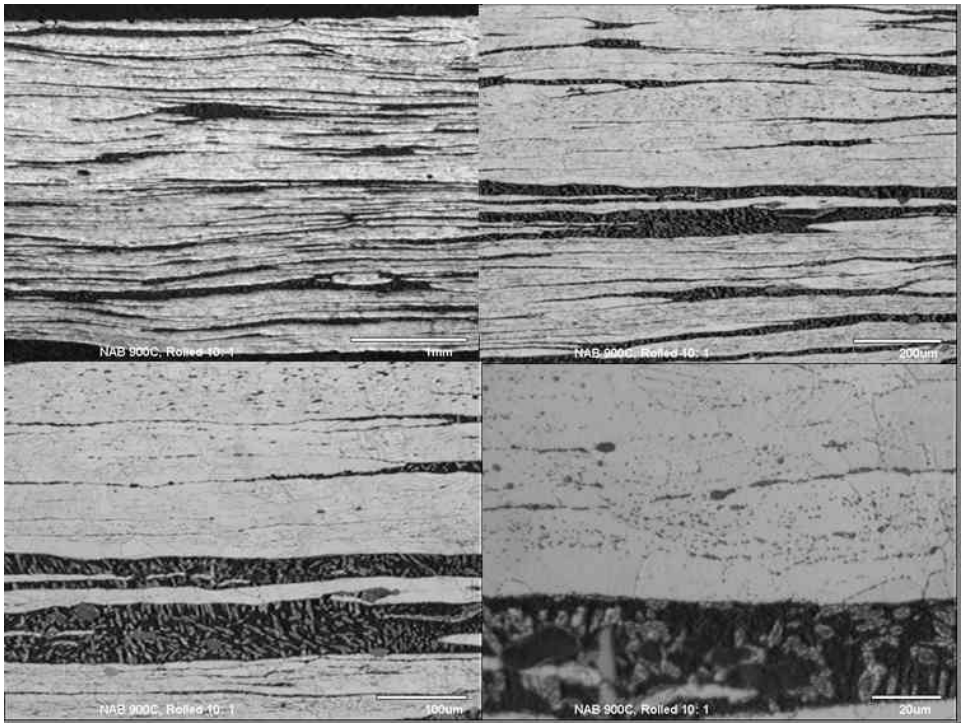

L. ROLLED 10 : 1 REDUCTION, 950 C – AIR COOLED

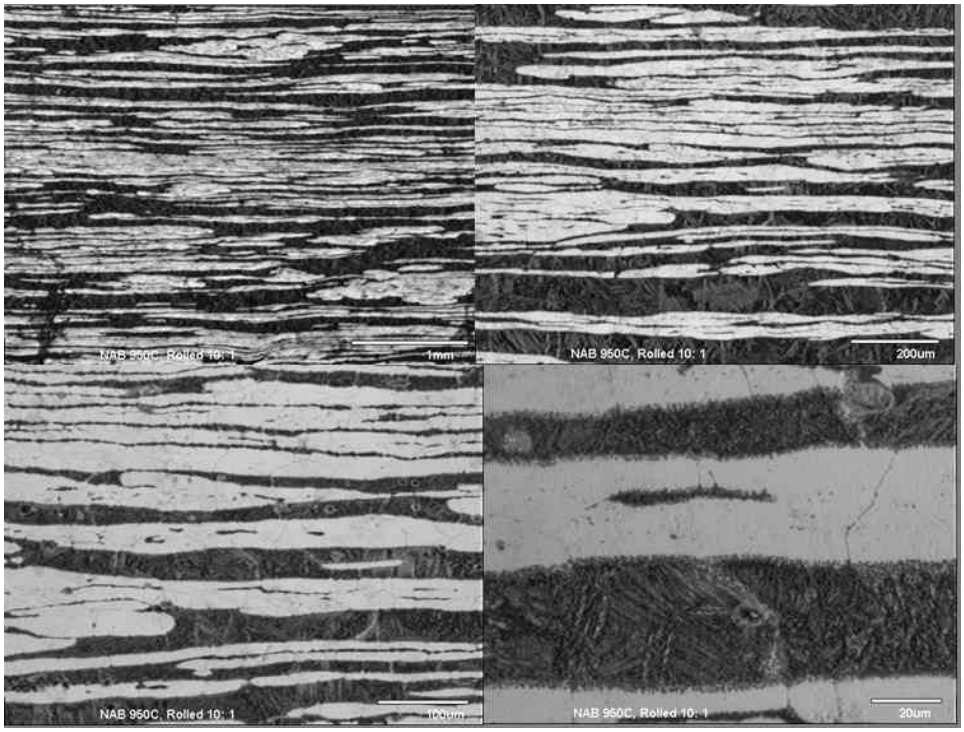

M. ROLLED 10 : 1 REDUCTION, 1000 C – AIR COOLED

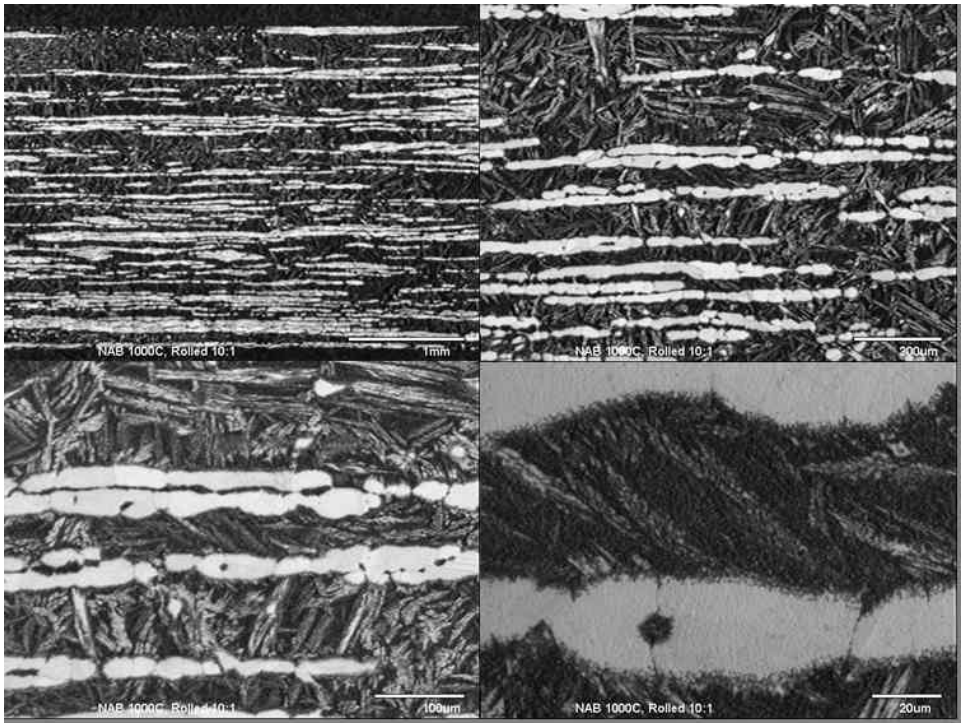

THIS PAGE INTENTIONALLY LEFT BLANK

APPENDIX B – MECHANICAL TEST DATA

A. TABULAR HARDNESS RESULTS

Macrohardness Tabular Results

Condition	Avg. Reading Rockwell 'B'-scale
As Cast	69.2
Annealed	
870	78.5
900	82.6
950	87.5
1000	90.4
3.5 : 1 Reduction	
870	94.6
900	87.6
950	94
1000	87.2
10 : 1 Reduction	
870	95
900	80.6
950	93.2
1000	89

Microhardness Tabular Results

Condition	Avg. Reading Vickers DPH
As Cast	141.22
Annealed	
870	165.44
900	196.21
950	200.04
1000	176.21
3.5 : 1 Reduction	
870	198.04
900	222.66
950	197.74
1000	202.53
10 : 1 Reduction	
870	225.28
900	178.78
950	206.99
1000	213.39

B. TENSILE TEST TABULAR RESULTS

1. Yield Strength (0.2% offset) Tabular Results

YS Data (MPa)

	Mean	Min	Max	Median	Deviation
As Cast	164.368	159.5	169.31	164.17	4.011063
870	202.445	196.67	205.99	199.56	7.974473
900	225.3124	215.85	237.047	225.84	9.118812
950	226.408571	209.42	236.28	214.57	12.60119
1000	242.4622	234.01	254.351	240.37	8.171127
870 s3.5	385.7625	329.9	430.05	391.55	41.89078
900 s3.5	348.54125	330.15	374.93	344.5425	18.95891
950 s3.5	349.3425	296.25	380.3	360.41	38.84647
1000 s3.5	273.538333	258.76	295.37	266.485	19.29728
870 s10	428.745	418.28	436.45	430.125	7.587343
900 s10	281.72725	249.164	306.395	285.675	23.86696
950 s10	314.057667	312.65	315.833	313.69	1.623039
1000 s10	316.8375	300.15	335.95	315.625	14.69106

2. Ultimate Tensile Strength Tabular Results

UTS Data (MPa)

	Mean	Min	Max	Median	Deviation
As Cast	372.6245	320.568	411.5403	360.1649	37.47921
870	427.5722	393.0151	455.4833	436.2961	22.19764
900	458.8772	431.0115	484.0789	463.4498	20.71751
950	452.38	415.7989	498.584	461.9469	29.60388
1000	449.7342	399.2946	475.6382	460.9364	32.24742
870 s3.5	573.6043	545.6454	632.5401	558.1158	39.74256
900 s3.5	552.0713	489.0027	623.5826	547.8499	55.91985
950 s3.5	537.7	474.6117	583.2852	546.4515	47.70482
1000 s3.5	581.029	448.4235	652.6281	611.5322	90.82234
870 s10	595.4663	495.0175	656.0508	615.3984	71.22631
900 s10	531.542	503.8006	558.4221	531.9726	26.01346
950 s10	643.91	639.1082	648.0051	644.6168	4.490362
1000 s10	687.7973	627.7765	718.572	702.4204	41.32329

3. Ductility Tabular Results

DUCTILITY DATA

	Mean	Min	Max	Median	Deviation
As Cast	10.750%	4.540%	23.120%	8.800%	6.590%
870	7.270%	5.960%	8.700%	7.600%	1.020%
900	6.750%	5.900%	7.540%	6.810%	0.640%
950	6.340%	5.880%	7.200%	6.180%	0.480%
1000	6.340%	5.880%	6.940%	6.200%	0.390%
870 s3.5	4.760%	3.880%	6.480%	4.340%	1.200%
900 s3.5	7.660%	3.180%	12.830%	7.320%	4.030%
950 s3.5	6.400%	5.380%	8.240%	6.000%	1.260%
1000 s3.5	28.970%	25.215%	35.683%	26.011%	5.828%
870 s10	8.620%	6.040%	13.050%	7.700%	3.070%
900 s10	18.870%	14.190%	24.310%	18.500%	4.190%
950 s10	29.040%	23.790%	34.250%	29.090%	5.230%
1000 s10	28.990%	26.620%	30.320%	29.520%	1.720%

THIS PAGE INTENTIONALLY LEFT BLANK

LIST OF REFERENCES

1. W. M. Thomas et. al.: 'Friction Stir Butt Welding,' International Patent Appl. No. PCT/GB92/02203 and GB Patent Appl. No. 9125978.8, Dec 1991, U.S. Patent No. 5,460,317 – from [Ref. 2] in support of information by Stephan Kallee and Dave Nicholas TWI.

2. Rhodes, C. G. et al., "Effects of Friction Stir Welding on Microstructure of 7075 Aluminum," *Scripta Materialia*, v. 36, No. 1, p. 69-75, 1997.

3. Mishra, R.S. and Mahoney, M.W., "Friction Stir Processing: A New Grain Refinement Technique to Achieve High Strain Rate Superplasticity in Commercial Alloys," *Materials Science Forum,* v. 357-359, p. 507-514, 2001.

4. K.V. Jata and S.L. Semiatin, "Continuous Dynamic Recrystallization During Friction Stir Welding of High Strength Aluminum Alloys," *Scripta Materialia*, v. 43, p. 743-749, 2000.

5. Sahoo, M., "Structure and Mechanical Properties of Slow-Cooled Nickel-Aluminum Bronze Alloy C95800," *AFS Trans*, v. 90, p. 913-926, 1982.

6. Culpan, E.A. and Rose, G., "Corrosion Behaviour of Cast Nickel Aluminium Bronze in Sea Water," *British Corrosion Journal,* v. 14, p. 160-166, 1979.

7. American Society for Testing and Materials (ASTM) B148 – 93a, Standard Specification for Aluminum-Bronze Sand Castings.

8. Sahoo, M., "Weldability of Nickel-Aluminum Bronze Alloy C95800," *AFS Trans*, v. 112, p. 893-911, 1982.

9. Wenschot, P., "The Properties of Ni-Al Bronze Sand Cast Ship Propellers in Relation to Section Thickness," *International Shipbuilding Progress*, v. 34, p.112-123, 1987.

10. F. Hasan, A. Jahanafrooz, G.W. Lorimer and N. Ridley, "The Morphology, Crystallography, and Chemistry of Phases in As-Cast Nickel-Aluminum Bronze," *Met. Trans A*, v. 13a, p.1337-1345, 1982.

11. A. Jahanafrooz, F. Hasan, G.W. Lorimer and N. Ridley, "Microstructural Development in Complex Nickel-Aluminum Bronze," *Met. Trans A*, v. 14a, p. 1951-1956, 1983.

12. D.M. Lloyd, G.W. Lorimer and N. Ridley, "Characterization of Phases in a Nickel-Aluminium Bronze," *Metals Technology*, v. 7, p. 114-119,

13. Culpan, E.A. and Rose, G., "Microstructural Characterization Of Cast Nickel Aluminium Bronze," *Journal of Materials Science*, v. 13, p. 1647-1657, 1978.

14. Brezina, P, "Heat Treatment of Complex Aluminum Bronzes," *Int. Met. Rev*., v. 27, n. 2, p. 77-120, 1982.

15. Weston, G.M., "Survey of Nickel-Aluminium-Bronze Casting Alloys on Marine Applications," Australia Dept. of Defence Report, DSTO MRL, Melbourne, Victoria, MRL-R-807, 1981.

16. Metals Handbook, 9th Ed., v. 2, Properties & Selections: Nonferrous Alloys and Pure Metals.

17. B. K. Vasquez, Master's Thesis, "The Effects of Isothermal Deformation and Annealing on the Microstructure of Nickel-Aluminum Bronze in Relation to the Friction Stir Process," Naval Postgraduate School, Monterey, CA, Dec 2002.

18. J. Sherburn, "Isothermal Annealing and Quenching Study," Naval Postgraduate School, Monterey, CA, AUG 2003

INITIAL DISTRIBUTION LIST

1. Defense Technical Information Center
   Ft. Belvoir, Virginia

2. Dudley Knox Library
   Naval Postgraduate School
   Monterey, California

3. Professor Terry McNelley
   Naval Postgraduate School
   Monterey, California

4. Murray W. Mahoney
   Rockwell Science Center
   Thousand Oaks, California

5. William Palko
   Naval Surface Warfare Center
   Carderock Division
   West Bethesda, Maryland

6. Dr. Leo Christodoulou
   DARPA/DSO
   Arlington, Virginia